Vertical profiles of global tropospheric nitrogen dioxide (NO₂) obtained by cloud-slicing TROPOMI

Rebekah P. Horner[1], Eloise A. Marais[1], Nana Wei[1], Robert G. Ryan[1,*], Viral Shah[2,3]

[1]Department of Geography, University College London, London, UK
[2]Global Modeling and Assimilation Office (GMAO), NASA Goddard Space Flight Center, Greenbelt, MD 20770, USA
[3]Science Systems and Applications, Inc., Lanham, MD 20706, USA
[*]Now at: School of Geography, Earth and Atmospheric Sciences, University of Melbourne, Melbourne, Australia

Correspondence to: Eloise A. Marais (e.marais@ucl.ac.uk); Rebekah P. Horner (rebekah.horner.20@ucl.ac.uk)

Abstract. Routine observations of the vertical distribution of tropospheric nitrogen oxides ($NO_x \equiv NO + NO_2$) are severely lacking, despite the large influence of NO_x on climate, air quality, and atmospheric oxidants. Here we derive vertical profiles of global seasonal mean tropospheric NO_2 by applying the cloud-slicing method to TROPOspheric Monitoring Instrument (TROPOMI) columns of NO_2 retrieved above optically thick clouds. The resultant NO_2 are at a horizontal resolution of $1° \times 1°$ for multiple years (June 2018 to May 2022) covering 5 layers in the upper (180-320 hPa and 320-450 hPa) and mid (450-600 hPa and 600-800 hPa) troposphere, and the marine boundary layer (800 hPa to the Earth's surface). Terrestrial boundary layer NO_2 are obtained as the difference between TROPOMI tropospheric columns and the integrated column of cloud-sliced NO_2 in all layers above the boundary layer. Cloud-sliced NO_2 is typically 20-60 pptv throughout the free troposphere and spatial coverage ranges from > 60% in the mid-troposphere to < 20% in the upper troposphere and boundary layer. Our product is similar (within 10-15 pptv) to NO_2 data from NASA DC-8 aircraft campaigns (INTEX-A, INTEX-B, ARCTAS, SEAC⁴RS, ATom) when both datasets are abundant and sampling coverage is commensurate, but such instances are rare. We use the cloud-sliced NO_2 to critique current knowledge of the vertical distribution of global NO_2, as simulated with the GEOS-Chem chemical transport model updated to include peroxypropionyl nitrate (PPN) and aerosol nitrate photolysis that liberate NO_2 in the lower and mid-troposphere for aerosol nitrate photolysis and upper troposphere for PPN. Multiyear GEOS-Chem and cloud-sliced means are compared to mitigate the influence of interannual variability. We find that for cloud-sliced NO_2 the interannual variability is ~10 pptv over remote areas and ~25 pptv over areas influenced by lightning and surface sources. The model consistently underestimates NO_2 across the remote marine troposphere by ~15 pptv. In the northern midlatitudes, GEOS-Chem overestimates mid-tropospheric NO_2 by 20-50 pptv, as NO_x production per lightning flash is parameterised to be almost double the rest of the world. There is a critical need for in-situ NO_2 measurements in the tropical terrestrial troposphere to evaluate cloud-sliced NO_2 there. The model and cloud-sliced NO_2 discrepancies identified here need to be investigated further to ensure confident use of models to understand and interpret factors affecting the global distribution of tropospheric NO_x, ozone and other oxidants.

Deleted: slicing

1 Introduction

In the troposphere, nitrogen oxides ($NO_x \equiv NO + NO_2$) influence the formation of tropospheric ozone (O_3), a greenhouse gas, and the hydroxyl radical (OH), the main atmospheric oxidant (Atkinson, 2000; Bloss et al., 2005). Due to its influence on OH, NO_x also indirectly affects the lifetime and abundance of the potent greenhouse gas methane (Wild et al., 2001) and non-methane volatile organic compounds that contribute to O_3 and particulate matter pollution (Crutzen and Andreae, 1990; Karl et al., 2007; Marais et al., 2016). NO_x is directly emitted from high-temperature combustion of fossil fuels, from open and domestic burning of biomass, and from natural processes such as lightning and bacteria in soils (Dignon, 1992; Pickering et al., 1998; Jain et al., 2006; Vinken et al., 2014). NO_x also enters the upper layers of the troposphere via downwelling from the stratosphere (Poulida et al., 1996). The distribution of NO_x varies throughout the troposphere as a result of these sources and due to recycling of NO_x via oxidation, photolysis and thermal decomposition of gas- and aerosol-phase reservoirs of nitrogen (Chatfield, 1994; Moxim et al., 1996; Kotamarthi et al., 2001; Scharko et al., 2014). In the warm lower troposphere where anthropogenic sources dominate, the lifetime of NO_x is a few hours. This increases with altitude to several days in the cold, dry upper troposphere where NO_x is present mostly as NO (Travis et al., 2016), reservoir compounds dominate, and terminal loss of NO_x via wet deposition in the form of nitric acid (HNO_3) is limited (Jaeglé et al., 1998).

Knowledge of the vertical distribution of tropospheric NO_x has been largely informed by in-situ instruments on research and commercial aircraft (Crawford et al., 1996; Brenninkmeijer et al., 1999; Bradshaw et al., 2000; Emmons et al., 2000; Petzold et al., 2015; Stratmann et al., 2016). These aircraft campaigns are few in time and space. The instruments used to measure NO_2 are also susceptible to interference from decomposition of thermally unstable reservoir compounds of NO_x (Bradshaw et al., 2000; Browne et al., 2011; Reed et al., 2016). This interference is most severe in the upper troposphere and in remote marine regions where thermally labile NO_x reservoir compounds are abundant and decomposition of these compounds is promoted by the warm instrument inlet (Murphy et al., 2004; Nault et al., 2015; Shah et al., 2023). Studies now supplement these measurements with calculated daytime NO_2 concentrations, as NO and NO_2 can be assumed to be in photochemical steady state (PSS) (Davis et al., 1993; Crawford et al., 1996).

Networks of ground-based remote sensing instruments such as Multi Axis Differential Optical Absorption Spectroscopy (MAX-DOAS) and direct-sun Pandora instruments have expanded globally. Still, geographic coverage for both is mostly in the northern hemisphere (Verhoelst et al., 2021). For Pandora, only the total tropospheric column can be derived from total atmospheric column measurements (Pinardi et al., 2020). MAX-DOAS, under ideal conditions, can retrieve up to four independent layers in the troposphere, though vertical extent at most sites excludes the upper troposphere (Tirpitz et al., 2021). Space-based remote sensing observations used to retrieve vertical column densities (VCDs) of tropospheric NO_2 address limited spatial sampling of commercial and research aircraft and Pandora and MAX-DOAS networks by offering daily global coverage, but with only one piece of vertical information in the troposphere (Ryan et al., 2023). These satellite observations

are also impacted by biases in modelled vertical profiles of NO_2 required to retrieve VCDs (Verhoelst et al., 2021), in particular in the upper troposphere where satellite observations are most sensitive to tropospheric NO_2 (Boersma et al., 2004; Travis et al., 2016; Silvern et al., 2018; Shah et al., 2023).

70   Mixing ratios of NO_2 in distinct layers of the troposphere can be retrieved using so-called cloud-slicing. This technique targets partial columns (stratospheric + tropospheric) above clouds that are sufficiently optically thick that UV-visible instruments observe discrete layers in the troposphere. Cloud-slicing was first applied by Ziemke et al. (2001) to O_3 columns to derive seasonal multi-year mean upper tropospheric O_3 mixing ratios in the tropics. Cloud-slicing has since been used to retrieve seasonal mean concentrations of NO_2 from the Ozone Monitoring Instrument (OMI) in both the mid (900-650 hPa or 2-4 km)

75   and upper (450-280 hPa or 6-11 km) troposphere at 5° latitude × 8° longitude (500 km × 800 km) as well as in six pressure levels (centred at 280, 380, 500, 620, 720 and 820 hPa) at 2° × 2° (Choi et al., 2014; Belmonte Rivas et al., 2015; Marais et al., 2018). The OMI cloud-sliced NO_2 data provide useful information at very coarse scales (20° × 32°, seasonal) (Marais et al., 2018) and are hindered by large data loss after 2007 when many satellite pixels became obscured by the row anomaly (Torres et al., 2018). More recently, the higher spatial resolution TROPOspheric Monitoring Instrument (TROPOMI) has been

80   used to derive NO_2 mixing ratios in the upper troposphere (450-180 hPa or 6-12 km) at finer scales than was possible with OMI of 1° × 1° (~100 km) (Marais et al., 2021). Cloud-sliced NO_2 from TROPOMI has so far only been derived for a single year, as at the time there were frequent updates to the retrieval that led to inconsistencies in the TROPOMI NO_2 VCDs used for cloud slicing. TROPOMI NO_2 data have since been reprocessed to obtain a consistent data record starting in May 2018.

85   Evaluation of cloud-sliced NO_2 data products is very limited, as coincidence of satellite observations and aircraft campaigns is rare. Choi et al. (2014) found that the NASA OMI mid tropospheric product is similar (<10% difference) to coincident research aircraft campaign observations, limited to Texas and the Pacific Ocean west of North America. Marais et al. (2021) intercompared seasonal mean cloud-sliced upper tropospheric NO_2 from TROPOMI and the NASA OMI product to identify that TROPOMI background values routinely exceed OMI by 12-26 pptv. Given these product disparities, independent

90   evaluation of cloud-sliced NO_2 mixing ratios is crucial. Past (2006-2013) NASA DC-8 aircraft campaigns and the more recent (2016-2018) NASA DC-8 Atmospheric Tomography Mission (ATom) measurement campaign sampled the troposphere from close to the surface to the upper layers of the troposphere, offering the opportunity to evaluate cloud-sliced NO_2 mixing ratios over the remote Pacific and Atlantic Oceans (ATom) (Thompson et al., 2022), the Canadian Arctic during the Arctic Research of the Composition of the Troposphere from Aircraft and Satellites (ARCTAS) campaign (Jacob et al., 2010), the eastern US

95   during the Intercontinental Chemical Transport Experiment – North America Phases A and B (INTEX-A and INTEX-B) (Singh et al., 2006, 2009) and the Studies of Emissions and Atmospheric Composition, Clouds and Climate Coupling by Regional Surveys (SEAC⁴RS) (Toon et al., 2016) campaigns, and the northern Pacific during INTEX-B.

Here we derive a global dataset of 4 years of seasonal multiyear mean concentrations of NO_2 in five discrete vertical layers in the troposphere from the planetary boundary layer to the upper troposphere. We evaluate our dataset against directly measured and calculated (PSS) NO_2 from multiple NASA DC-8 aircraft campaigns and go on to use the cloud-sliced data to assess current understanding of the global vertical distribution of tropospheric NO_x as simulated by the GEOS-Chem chemical transport model.

2 Methods

2.1 Cloud-slicing TROPOMI NO_2 columns

TROPOMI was launched in October 2017 aboard the Sentinel-5P satellite. The initial TROPOMI nadir spatial resolution of 7.2 km × 3.5 km was enhanced to 5.6 km × 3.5 km in August 2019 (Liu et al., 2021). The swath width is 2600 km, resulting in daily global coverage at an equator crossing time of 13:30 local solar time (LST). To derive our cloud-sliced product, we use TROPOMI Level 2 swaths retrieved using a consistent algorithm (version 2.3.1). Data are available as the reprocessed (PAL) product from 1 June 2018 to 14 November 2021 (https://data-portal.s5p-pal.com/, last accessed 17th February 2022) and as the offline (OFFL) product from 14 November 2021 to 31 May 2022 (https://s5phub.copernicus.eu/dhus/#/home, last accessed 7 July 2022; now available at https://dataspace.copernicus.eu/browser/). The cloud-slicing approach was first applied to TROPOMI by Marais et al. (2021) to derive NO_2 mixing ratios in the upper troposphere over a broad pressure range from 450 to 180 hPa. We apply this cloud-slicing, with updates detailed below, to the whole troposphere to derive vertical profiles of seasonal mean NO_2 at the same 1° × 1° resolution as Marais et al. (2021) for multiple years (2018-2022) over five pressure ranges: one in the boundary layer below 800 hPa (< ~2 km), two in the mid-troposphere at 800-600 hPa (~2-4 km) and 600-450 hPa (~4-6 km), and two in the upper troposphere at 450-320 hPa (~6-9 km) and 320-180 hPa (~9-12 km).

The first application of cloud-slicing to TROPOMI NO_2 is described in detail in Marais et al. (2021). We mostly follow the same approach. That is, pixels of individual swaths are filtered to isolate observations above optically thick clouds (cloud radiance fraction > 0.7). These are binned into cloud-top pressures within the 5 targeted pressure ranges on a fixed 1° × 1° grid. The stratospheric component of the total VCDs is corrected for a 13% underestimate in variance identified by Marais et al. (2021) from comparison to ground-based direct sun photometer Pandora measurements at the high-altitude (4.2 km) Mauna Loa site. The corrected stratospheric VCDs are multiplied by the reported stratospheric air mass factors (AMFs) to calculate stratospheric slant columns. The stratospheric slant columns are then subtracted from the total slant columns to estimate tropospheric slant columns that are converted to tropospheric VCDs using a geometric AMF. Only clusters of total above-cloud VCDs with a relatively uniform stratosphere are retained for cloud-slicing. These are identified as clusters of 1° × 1° pixels with a stratospheric column relative standard deviation < 0.02. A uniform stratosphere ensures that variability in partial NO_2 columns above optically thick clouds is dominated by variability in the troposphere. Cloud-slicing also requires that each

cluster include a representative range of cloud-top pressures (Choi et al., 2014). To ensure this is achieved, we remove clusters with cloud pressure ranges that are < 60% of the pressure range of each layer (for example, 120 hPa threshold for the 800-600 hPa layer) and that have a large standard deviation ($\geq$ 30 hPa), which is consistent with cloud-slicing by Choi et al. (2014) and

135 Marais et al. (2018, 2021).

Next, we regress cloud-top pressures against above-cloud NO_2 VCDs for clusters with at least 10 satellite pixels. We replace the reduced major axis (RMA) regression fit originally used by Marais et al. (2021) with Theil regression, as this reduces influence from outliers and is better suited to data that are not always normally distributed (Theil, 1950; Sen, 1968). The

140 regression slope in molecules cm^{-2} hPa^{-1} is converted to NO_2 volume mixing ratios in pptv as in Equation (5) of Choi et al. (2014). The updated Theil regression fit addresses the 12-26 pptv overestimate in background values of cloud-sliced upper tropospheric NO_2 identified by Marais et al. (2021) from comparison to the OMI upper tropospheric product. It also negates the need for the large TROPOMI free tropospheric column NO_2 bias correction that Marais et al. (2021) used to resolve an apparent overestimate in TROPOMI compared to free tropospheric NO_2 columns derived with measurements from Pandora

145 and MAX-DOAS instruments at the high-altitude Izaña site. We also find that the outlier filter used by Marais et al. (2021) for cloud-sliced NO_2 > 200 pptv is no longer needed, as it has negligible impact on seasonal mean cloud-sliced NO_2 using our updated approach. As an initial assessment, we compare upper tropospheric cloud-sliced NO_2 from our updated cloud-sliced approach to those from Marais et al. (2021). To ensure a consistent comparison, we recompute our updated cloud-sliced NO_2 to cover the same pressure range (450-180 hPa) and time (June 2019 to May 2020) as Marais et al. (2021) and only compare

150 $1° \times 1°$ grids with 5 or more cloud-sliced data points in each data product.

The use of a geometric AMF to convert slant columns to vertical columns assumes the vertical distribution of NO_2 within each layer is relatively constant. Belmonte Rivas et al. (2015) estimated that the difference between the geometric AMF and an AMF that accounts for surface reflectivity, the vertical NO_2 profile and atmospheric scattering is <10% in all layers, except

155 the lowest layer in that work of 770-870 hPa. In this lowest layer, equivalent to the top half of the boundary layer in our work, the difference in AMFs is up to ~30%. The largest differences occur over land where NO_x emissions from sources such as urban traffic, industry, soils, and open burning of biomass cause an exponential increase in NO_2 with pressure, unlike over the oceans where the NO_2 profile is relatively uniform (Schreier et al., 2015; Wang et al., 2019; Kang et al., 2021; Shah et al., 2023). Given the steep vertical gradient in terrestrial boundary layer NO_2, we instead derive NO_2 mixing ratios in the lowest

160 layer over terrestrial regions as the difference between TROPOMI seasonal mean cloud-free NO_2 tropospheric columns and free tropospheric columns obtained by integrating cloud-sliced NO_2 over the four layers above the boundary layer (800-180 hPa) where data are available in all four overlying layers.

Cloud fraction and cloud-top height data are from the improved Fast Retrieval Scheme for Clouds from the Oxygen A-band

165 wide (FRESCO) algorithm called FRESCO-wide (Eskes and Eichmann, 2023). FRESCO-wide minimises the difference

between measured and simulated spectra between 757-758, 760-761 and 765-770 nm and is so-called because the third spectral window is wider than the 765-766 nm window used in the previous FRESCO-S algorithm (Wang et al., 2008; Van Geffen et al., 2022). The cloud-top pressure retrieved with FRESCO-wide corresponds to an altitude ~1 km lower than the physical cloud-top height, as the cloud-top height retrieval assumes clouds are uniform reflective boundaries (Choi et al., 2014; Loyola et al., 2018). Marais et al. (2021) showed that cloud-sliced NO_2 is relatively insensitive to the choice of TROPOMI cloud product. Their use of the TROPOMI Retrieval of Cloud Information using Neural Networks Cloud As Layers (ROCINN-CAL) product yielded upper tropospheric NO_2 that was only 4-9 pptv more than that from the FRESCO-S product. The small difference results from an extratropical latitude-dependent divergence in cloud-top heights between the two products. The reprocessed TROPOMI NO_2 product (v2.3.1) includes data from two cloud retrieval algorithms, FRESCO-wide and O_2-O_2 cloud (O22CLD). FRESCO-wide is used here, as we find that it yields greater data density than the O22CLD product and differences in NO_2 between the two products for coincident grids are small (< 10%). As of August 2023, ROCINN-CAL had not been reprocessed to obtain a consistent record, so is not used.

2.2 NASA DC-8 aircraft observations used to evaluate cloud-sliced NO_2

We evaluate our cloud-sliced NO_2 against NASA DC-8 campaign data. To mitigate interference from decomposition of NO_x reservoir compounds on measured NO_2 over remote regions, we calculate PSS NO_2 for ATom measurements over remote oceans and for all measurements made in the upper troposphere. The PSS NO_2 calculation assumes a dynamic daytime equilibrium between NO and NO_2 resulting from the balance between photolysis of NO_2 yielding NO and reaction of NO with oxidants regenerating NO_2. Silvern et al. (2018) estimated with GEOS-Chem that oxidation of NO in the southeast US upper troposphere was mostly (75%) by O_3 followed by the hydroperoxy radical (HO_2) (15%). The remaining 10% is due to oxidation by the methyl peroxy radical (CH_3O_2) and halogen monoxides. Given dominance of O_3 and HO_2 and availability of measurements of these for almost all campaigns used, we calculate PSS NO_2 as follows:

$$NO_2 = NO \times \left(\frac{k_1[O_3] + k_2[HO_2]}{j_{NO_2}} \right)$$ (1),

where j_{NO_2} is the NO_2 photolysis frequency (in s^{-1}) and k is the rate constant for oxidation of NO by O_3 (k_1) and by HO_2 (k_2) (in cm^3 $molecule^{-1}$ s^{-1}). The square brackets denote concentrations of O_3 and HO_2 in molecules cm^{-3}. NO and NO_2 are in pptv. Values of j_{NO_2}, NO, [O_3], and [HO_2] are from direct measurements and k_1 and k_2 are calculated using the temperature-dependent Arrhenius equations documented in the Jet Propulsion Laboratory (JPL) Chemical Kinetics and Photochemical Data publication number 19 (Burkholder et al., 2020). These for cold upper tropospheric temperatures (~220 K) are $k_1 = 1.2 \times 10^{-14}$ cm^3 $molecule^{-1}$ s^{-1} and $k_2 = 1.1 \times 10^{-13}$ cm^3 $molecule^{-1}$ s^{-1}. Only aircraft data obtained between 12:00 and 15:00 LST, 1.5 hours around the TROPOMI overpass time of 13:30 LST, are used, to ensure consistent sampling of the midday atmosphere

and that the PSS assumption is valid. We remove aircraft data influenced by stratospheric air, identified as $O_3/CO > 1.25$ mol mol^{-1}. We also only use aircraft NO data to calculate PSS NO_2 if the NO measured is double the NO instrument detection limit of 6 pptv. This ensures measurements used are distinct from background noise in our PSS calculation (Ryerson et al., 2000; Yang et al., 2023).

NASA DC-8 aircraft campaigns with direct observations of NO_2 and observations needed to calculate PSS NO_2 include INTEX-A in summer 2004 over the United States (Singh et al., 2006), INTEX-B in spring 2006 over the eastern US, the Gulf of Mexico and the northern Pacific Ocean (Singh et al., 2009), ARCTAS in spring and summer 2008 over the Canadian Arctic (ARCTAS Science Team, 2011), SEAC^{4}RS in summer and autumn 2013 over the southeast US (SEAC4RS Science Team, 2014), and ATom once in all seasons from 2016 to 2018 following the same pole-to-pole flight path over the Atlantic and Pacific Oceans (ATom Science Team, 2021). Direct NO_2 measurements are from thermal-dissociation laser induced fluorescence (TD-LIF) (Di Carlo et al., 2013) for INTEX-A and INTEX-B, and from chemiluminescence (Ryerson et al., 2000) for all other campaigns. There are other DC-8 aircraft campaigns, such as the Subsonic Assessment Ozone and NO_x Experiment (SONEX) over the North Atlantic and the Deep Convective Cloud and Chemistry (DC-3) over the eastern US. These are not included in our comparison, because SONEX has routine influence of stratospheric air (Fuelberg et al., 2000) and because DC-3 targeted thunderstorms with large concentrations of NO_x from lightning, so is not representative of a standard atmosphere (Singh et al., 1999; Barth et al., 2015; Nault et al., 2016). Measurements of HO_2 are not available for SEAC^{4}RS, so the PSS NO_2 calculation for this campaign uses average upper tropospheric $[HO_2]$ from the other three campaigns. We find that INTEX-A measurements of NO yield median PSS NO_2 values at 450-180 hPa that are anomalously large (150-450 pptv) in comparison to PSS NO_2 from SEAC^{4}RS (30-130 pptv), so no upper tropospheric (450-180 hPa) INTEX-A values are used.

2.3 The GEOS-Chem chemical transport model

We use GEOS-Chem to evaluate contemporary knowledge of tropospheric NO_x by comparison to our cloud-sliced NO_2 vertical profiles. For this, we use GEOS-Chem version 13.3.4 (https://doi.org/10.5281/zenodo.5764874; accessed 11 May 2022) to calculate 4-year seasonal mean NO_2 covering the same vertical ranges as cloud-sliced NO_2. Model years sampled (1 December 2015 to 30 November 2019) are different to those for TROPOMI, due to a lag in availability of emission inventory data. The model is driven with NASA Modern Era Retrospective analysis for Research and Applications, version 2 (MERRA-2) reanalysis meteorology at a horizontal resolution of $2° \times 2.5°$ over 47 vertical layers (30-35 in the troposphere) extending to 0.01 hPa.

Global emissions of all anthropogenic sources except aircraft are from the Community Emissions Data System (CEDS) version 2 for 2015 to 2019 (McDuffie et al., 2020). Aircraft emissions of NO_x are from the Aviation Emissions Inventory Code (AEIC) for 2005 (Stettler et al., 2011). We use offline grid-independent soil NO_x emissions from Weng et al. (2020), the online Global

Fire Emissions Database version 4 with small fires (GFED4s) (van der Werf et al., 2017) inventory for open burning of biomass, and offline grid-independent lightning NO_x emissions prepared by Meng et al. (2021) using the parameterisation detailed in Murray et al. (2012).

240 GEOS-Chem exhibits a known underestimate in tropospheric NO_2 over global oceans, as evidenced by past studies (Travis et al., 2020; Guo et al., 2023; Shah et al., 2023). We address this by updating the GEOS-Chem chemical mechanism to include photolysis of particle-phase nitrates (pNO_3) liberating NO_x as NO_2 and as the reservoir compound nitrous acid (HONO) followed by its prompt photolysis to form NO (Ye et al., 2017; Kasibhatla et al., 2018; Romer et al., 2018; Andersen et al., 2023). Photolysis of pNO_3 is implemented in GEOS-Chem by scaling the photolysis of nitric acid (HNO_3) by an enhancement

245 factor (EF). The EF is 100 for coarse-mode pNO_3 and is scaled down using the relative molar concentrations of pNO_3 and sea salt aerosol as in Shah et al. (2023) for fine-mode pNO_3. This increases lower tropospheric (< 6 km) NO_2 over the remote ocean by up to 15 pptv, but has a smaller effect (< 10 pptv increase) above 6 km where pNO_3 is much less abundant (Shah et al., 2023). Photolysis of the NO_x reservoir compound peroxypropionyl nitrate (PPN, $C_2H_5C(O)OONO_2$) leading to formation of NO_2 occurs in the atmosphere, but is absent in GEOS-Chem. There are no reported laboratory measurements of NO_2

250 quantum yields from PPN. According to the Harwood et al. (2003) laboratory study, PPN absorption cross sections and quantum yields of the nitrate radical (NO_3) are within 10% of peroxyacetyl nitrate (PAN, $CH_3C(O)OONO_2$), so we use PAN quantum yields and cross sections from Burkholder et al. (2020) to represent PPN photolysis in GEOS-Chem.

For consistent comparison of the model to cloud-sliced NO_2, GEOS-Chem is sampled around the TROPOMI overpass (12:00-

255 15:00 LST) following a 3-month spin-up from 1 September to 30 November 2015 for chemical initialisation of the 4-year simulation. Tropospheric NO_2 in GEOS-Chem is identified using MERRA-2 tropopause heights and additional filtering is applied to remove stratospheric intrusions (O_3/CO > 1.25 mol L^{-1}). All-sky model scenes are sampled. Marais et al. (2021) determined by applying cloud-slicing to synthetic columns of NO_2 simulated with GEOS-Chem that the difference between NO_2 under very cloudy and all-sky conditions is small (< 17%). The TROPOMI cloud-sliced data are gridded to the GEOS-

260 Chem grid for the comparison and only grid cells with at least 10 cloud-sliced data points are compared. We use a threshold of 10 to ensure that meaningful comparisons can be made between GEOS-Chem and cloud-slicing without excluding a large number of cloud-sliced data.

3 Results and Discussion

3.1 Vertical distribution of tropospheric NO_2 from cloud-slicing TROPOMI

265 Fig. 1 shows the spatial distribution of cloud-sliced NO_2 in the free troposphere in June-August (JJA) 2018-2021 and December-February (DJF) 2018-2022 and Fig. 2 shows boundary-layer NO_2 (below 800 hPa) for the same seasons and years obtained with cloud-slicing over the ocean and differencing over land (Sect. 2.1). The percent filled global $1° \times 1°$ grids is

similar in both seasons, though with expected seasonal shifts in regions covered, due to seasonality in the location of clouds associated with convective features such as the Intertropical Convergence Zone (ITCZ) and absence of clouds over regions of persistent subsidence west of southern Africa and South America. Coverage is greatest in the mid-troposphere and least at 320-180 hPa. Percent coverage averaged over JJA and DJF is 63% of grid cells for 600-450 hPa and 68% for 800-600 hPa covering most of the tropics, subtropics, and midlatitudes. Slightly fewer (38%) result at 450-320 hPa, decreasing to 8% at 320-180 hPa. The few grid squares that are filled at this height mostly occur in the tropics, due to the higher tropopause and greater abundance of optically thick clouds (Wang et al., 1996). In the boundary layer (Fig. 2), a total of ~14% of the grids are filled, ~11% for direct cloud-slicing and ~3% for differencing. The latter is limited to locations over land with cloud-sliced NO$_2$ in the top upper troposphere layer. Per-layer percent grids filled is similar for March-May and September-November.
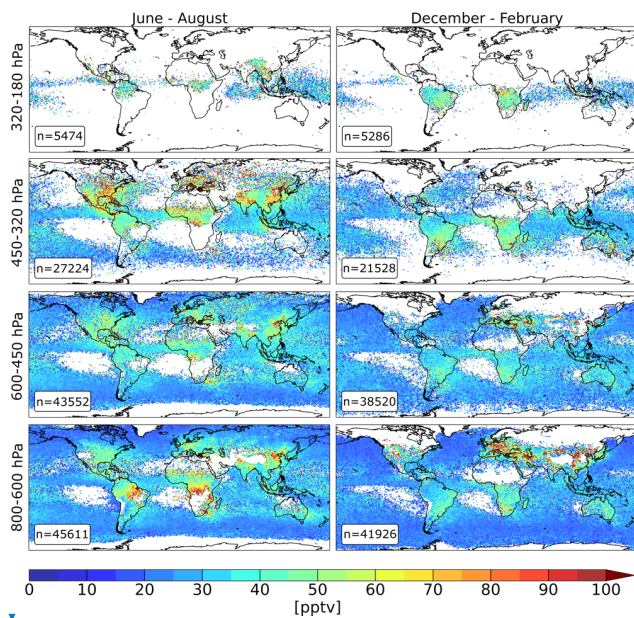
Figure 1: Seasonal mean NO$_2$ in the free troposphere obtained by cloud-slicing TROPOMI. Columns are June-August (JJA; left) and December-February (DJF; right) multiyear (2018-2021 for JJA, 2018-2022 for DJF) means at 1° × 1°. Rows from top to bottom are 320-180, 450-320, 600-450, and 800-600 hPa. Inset boxes give the number of filled 1° × 1° grids. Boundary layer (below 800 hPa) data are in Fig. 2.
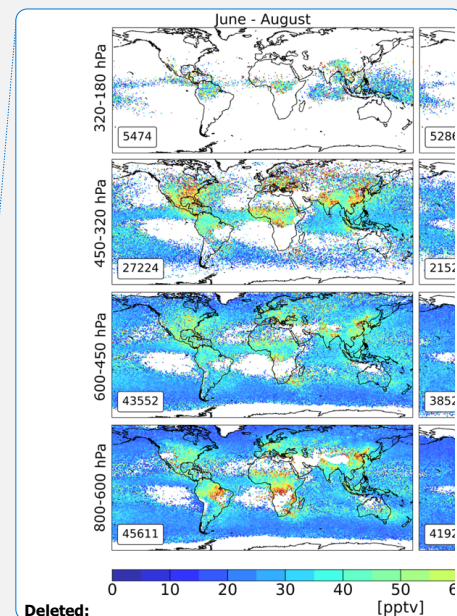
285 Throughout the free troposphere in all seasons (Fig. 1), cloud-sliced NO_2 is typically 20-60 pptv. In the upper troposphere, lightning NO_x emissions and photolysis of NO_x reservoir compounds sustains NO_2 concentrations of 20-70 pptv over the oceans and > 90 pptv over the continents in JJA at 450-320 hPa. NO_2 concentrations exceeding 70 pptv in JJA at 450-320 hPa over North America, China and the Indian subcontinent is due to a combination of lightning and convective uplift of surface anthropogenic pollution (Bertram et al., 2007; Hudman et al., 2007). NO_2 persists for longer in the cold, dry upper troposphere

290 (Ehhalt et al., 1992; Jaeglé et al., 1998; Grewe et al., 2001) than in the mid-troposphere below, so NO_2 concentrations are 20 pptv more over Europe and North America at 450-320 hPa than at 600-450 hPa. NO_2 over the open oceans is similar (25-50 pptv) throughout the free troposphere and is due mostly to lightning and continental outflow (Kawakami et al., 1997; Zien et al., 2014). NO_2 in excess of 55 pptv over South America and 80 pptv over Central Africa at 800-600 hPa results from a mix of intense continental lightning and seasonal open burning of biomass (Andreae et al., 2001; Christian et al., 2003; Duncan et

295 al., 2003). The burning season in South America starts in July and occurs throughout JJA in southern Africa and throughout DJF in Africa north of the tropics (Van Der Werf et al., 2006; Castellanos et al., 2014; Van Der Velde et al., 2021). NO_2 is longer-lived in winter, due to cold conditions and slow photolysis (Dickerson et al., 1982; Kenagy et al., 2018), so over continental Europe large surface sources of anthropogenic NO_x and limited lightning activity especially in comparison to the US contribute to 80 pptv more NO_2 in DJF than in JJA at 800-600 hPa.

300

Deleted:
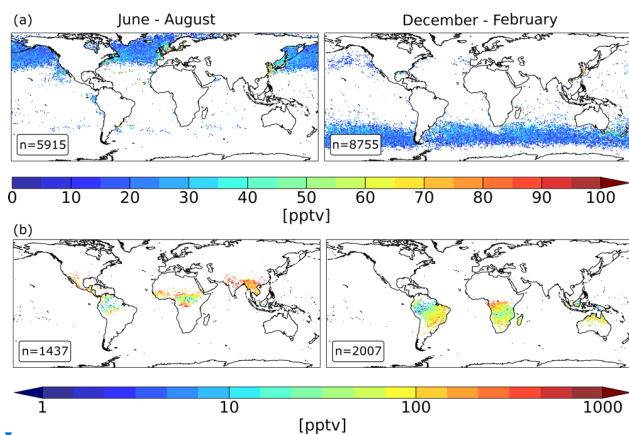
Figure 2: As in Fig. 1, but for the boundary layer (below 800 hPa). Panels are NO_2 from cloud-slicing over the oceans (a) and from the differencing approach over land (b) (see Sect. 2.1 for details). Note colourbar ranges differ in panels (a) and (b), and (b) is on a log scale.

305

In the marine boundary layer (Fig. 2 (a)), the typical range in NO_2 concentrations is similar to the layers above, except close to coastlines influenced by continental outflow of anthropogenic pollution and local NO_x production from busy harbours.
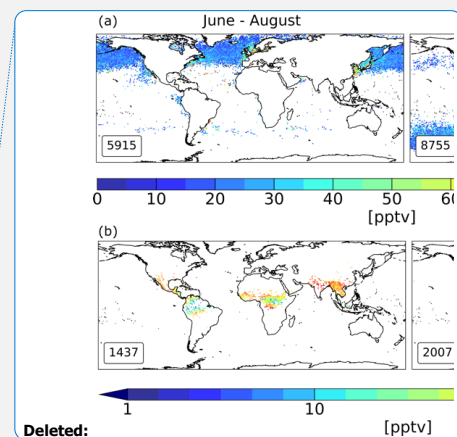
Along the east coast of China, for example, NO₂ concentrations are > 90 pptv compared to 25-35 pptv over the remote ocean east of China. Terrestrial boundary layer NO₂ coverage in Fig. 2 (b) is limited to the tropics in JJA and the tropics and southern subtropics in DJF where cloud-sliced NO₂ data are available in all 4 overlying layers (Fig. 1). In the terrestrial boundary layer, NO₂ concentrations exceed 30 pptv and peak at 600 pptv over eastern Brazil in DJF, Central Africa in both seasons and Southeast Asia and the Indo-Gangetic Plain (IGP) in JJA. The peaks in Brazil and Central Africa are due to biomass burning, whereas the peaks in Southeast Asia and the IGP are associated with large urban and industrial sources (Giglio et al., 2010; Ghude et al., 2013; Lu et al., 2024). Steep latitudinal gradients in NO₂ of > 100 pptv obtained with the differencing approach for NO₂ covering Amazonia and Central Africa is due to influence of intense seasonal burning of savanna-type vegetation bordering dense tropical forests (Chen et al., 2013; Ossohou et al., 2019; Jin et al., 2021; Van Der Velde et al., 2021).

The seasonal mean cloud-sliced NO₂ at 450-180 hPa obtained by Marais et al. (2021) that we compare to our data for the same vertical extent and time period (Sect. 2.1) ranges from NO₂ > 80 pptv over terrestrial regions to < 50 pptv over remote oceans. The two datasets are spatially consistent in all seasons, yielding Pearson's correlation coefficients (R) of 0.74 in JJA, 0.70 in SON, 0.64 in DJF and 0.65 in MAM. Marais et al. (2021) NO₂ is on average 26% more than we obtain with our updated cloud slicing. This difference, decomposed into variance and background using RMA regression, is 25-37% more variance and 17-22 pptv less background NO₂ in our data across all four seasons. The greater background values in Marais et al. (2021) are from susceptibility of their approach to outliers (Sect. 2.1).
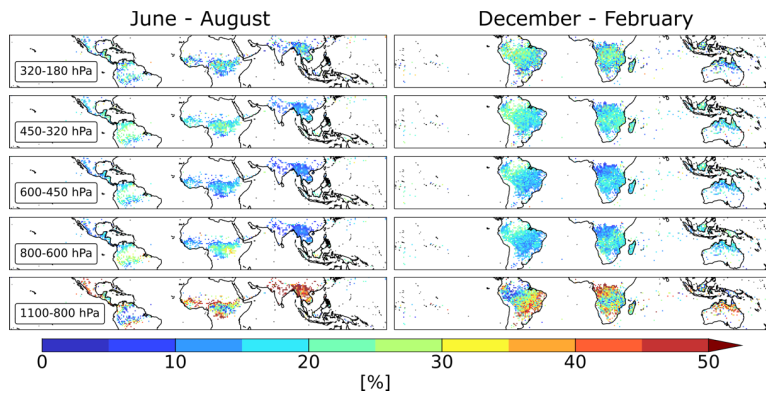
Figure 3: Seasonal mean percentage contribution of NO₂ each cloud-sliced layer to the tropospheric column. Columns are June-August (JJA; left) and December-February (DJF; right). Rows from top to bottom are 320-180, 450-320, 600-450, 800-600, and 1100-800 hPa. Data are multiyear means at 1° × 1°.

Fig. 3 shows the relative contribution of individual layers to the tropospheric column that is obtained by summing the column densities of cloud-sliced NO_2 in each layer for grid cells with data in all layers. This limits coverage to the tropics and subtropics. As expected, the boundary layer contribution is greatest, typically exceeding 55% in locations influenced by intensive anthropogenic activity and biomass burning (Sahu and Sheel, 2014; Beirle et al., 2019; Keita et al., 2021). The relative contribution from layers above the boundary layer exhibit zonal and meridional variability, but are relatively constant with altitude at ~20% over central Africa and ~10% over south Asia.

We also examine the size of interannual variability (IAV) in tropospheric NO_2, according to our cloud-sliced data. This is shown in Fig. 4 for JJA and DJF for a select year (2021 for JJA, December 2020 to February 2021 for DJF), calculated as the absolute difference between cloud-sliced NO_2 in these years and the multiyear mean (Fig. 1). Only three of the five layers are shown, as coverage is poor for individual years for the other two layers. IAV data are obtained for <1% of all 1° × 1° grid cells at 180-320 hPa and just 2% in the boundary layer. IAV in the layers shown in Fig. 4 is typically ~10 pptv over the remote ocean and ~25 pptv over continental regions (eastern US, Europe, tropics). The greater IAV over the continents is due to influence of anthropogenic, open biomass burning and lightning NO_x emissions. IAV NO_2 is about 20-50% of the variability the multiyear means in Fig. 1 and 2. Relatively large IAV NO_2 over the remote oceans is restricted to the edges of sampled areas in the subtropics that have low data density, due to the proximity to regions of persistent subsidence where retrievals from cloud-slicing are not always successful.
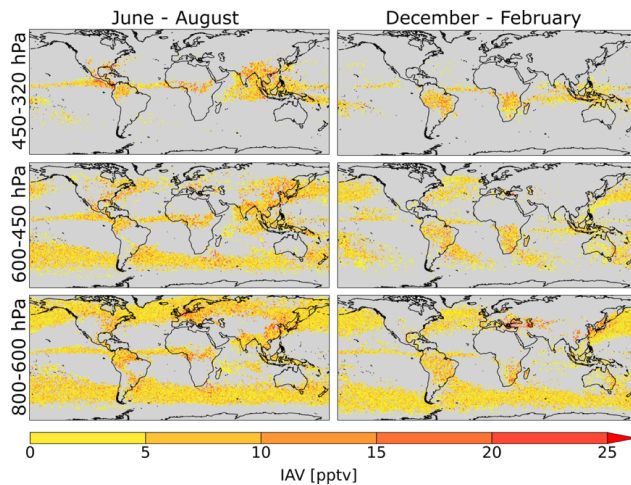
Figure 4: Free tropospheric NO₂ interannual variability (IAV). Panels are single-year NO₂ IAV obtained as the absolute difference between single-year (left: JJA 2021; right: DJF 2020-2021) and multiyear mean cloud-sliced NO₂ for the 3 layers with greatest geographic coverage. Only grid squares with at least 5 cloud-sliced data points in the single-year means are compared.

3.2 Evaluation of cloud-sliced NO₂ with observed and calculated (PSS) NO₂

Fig. 5 shows the regions selected to intercompare cloud-sliced and DC-8 NO₂ obtained with direct measurements and PSS NO₂ (Section 2.2). Selected regions include the North Atlantic Ocean sampled during ATom, the Canadian Arctic sampled during ARCTAS and ATom, the eastern United States sampled during SEAC⁴RS, INTEX-A and INTEX-B, and the Pacific Ocean sampled during ATom and INTEX-B. These regions were chosen to optimise coincidence of aircraft data in all five layers. In many instances, though, coincidence is over a limited extent of the sampling domain, especially the upper troposphere in almost all domains and the Pacific Ocean in all layers. Domains sampled in all seasons due to the ATom campaign include the Canadian Arctic and the Pacific and Atlantic Oceans. The most sampled time period is JJA, the greatest regional coverage is over the eastern US, and the mid-tropospheric layers (800-600 and 600-450 hPa) have the most DC-8 data. According to the DC-8 NO₂ data, hotspots (NO₂ > 200 pptv) occur over the US terrestrial boundary layer where there are large surface NOₓ emissions. Much lower concentrations of < 25 pptv over the remote ocean are due to absence of large local sources.
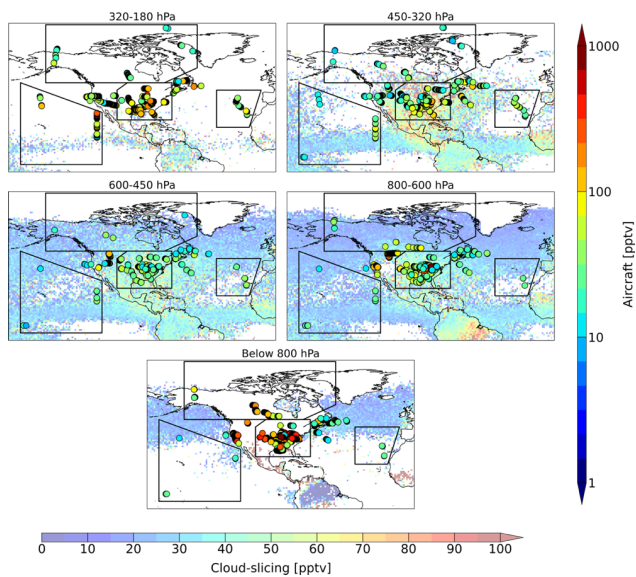
375

Figure 5: Maps of tropospheric NO$_2$ over the north-western hemisphere in June-August for the five cloud-slicing pressure ranges. Filled circles are DC-8 NO$_2$ data along DC-8 flight tracks (Sect. 2.2). Background values are cloud-sliced NO$_2$. Polygons show the regions sampled for comparison of aircraft and cloud-sliced NO$_2$ in Fig. 6 and 7. These are the North Atlantic, the Canadian Arctic, the eastern United States and the Pacific.

380

Fig. 6 and 7 compare median DC-8 and cloud-sliced NO$_2$ concentrations in MAM and JJA (Fig. 6) and SON and DJF (Fig. 7) for the polygons in Fig. 5. Cloud-slicing data are for 2018-2021 in JJA and SON, 2018-2022 in DJF, and 2019-2022 in MAM. JJA data are compared to the ARCTAS, SEAC^{4}RS, INTEX-A and ATom-1 campaigns, DJF to ATom-2, SON to ATom-3 and SEAC^{4}RS, and MAM to ATom-4, ARCTAS and INTEX-B across all layers except for INTEX-A which we do not use for

385 comparisons in the upper troposphere (450-180 hPa) (Sect. 2.2). Vertical profiles of DC-8 NO$_2$ are relatively stable (~25-80 pptv) throughout the troposphere over Pacific and North Atlantic Oceans and increase exponentially to ~75-450 pptv in the boundary layer over the southeastern US and the Canadian Arctic. Most cloud-sliced NO$_2$ in the mid-troposphere and in the 320-450 hPa layer in the upper troposphere are < 15 pptv different to DC-8 NO$_2$ in the extensively sampled southeastern US and < 25 pptv in the other locations for medians obtained with more than 5 data points. Greater variability in each layer (wider

390 interquartile ranges) in either dataset is typically because there are fewer data points and less extensive coverage (Fig. 4).
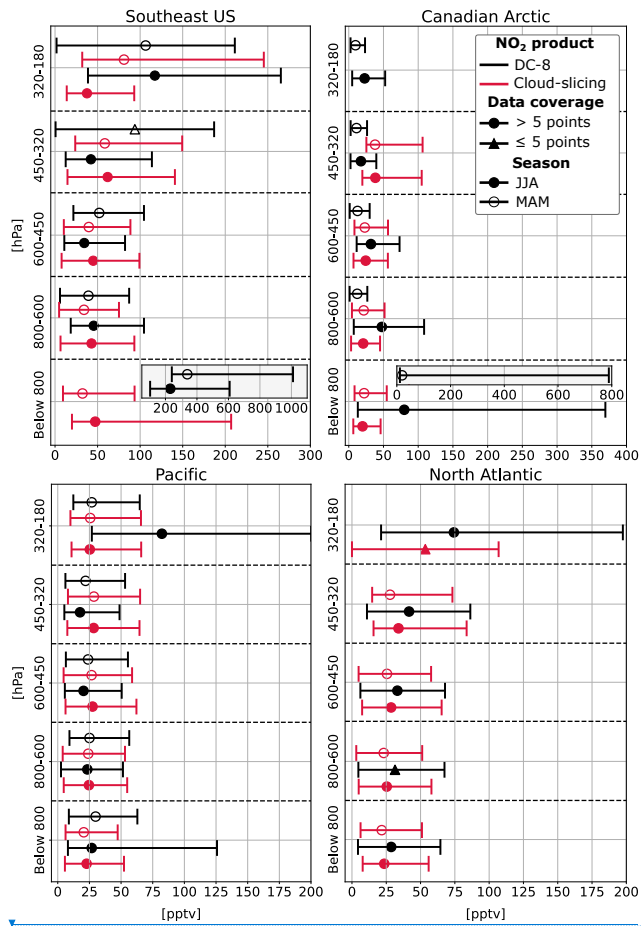
Figure 6: Comparison of seasonal mean vertical profiles of DC-8 and cloud-sliced tropospheric NO₂. Symbols are median values for the sampling domains in Fig. 5 for data in MAM (open) and JJA (filled). Symbol shapes for both DC-8 and cloud-slicing datasets differentiate medians obtained with ≤ 5 (triangle) and > 5 (circle) data points. Error bars are interquartile ranges (IQR). NO₂ concentration scales differ and inset boxes in the top row show boundary-layer NO₂ exceeding the *x*-axis range.
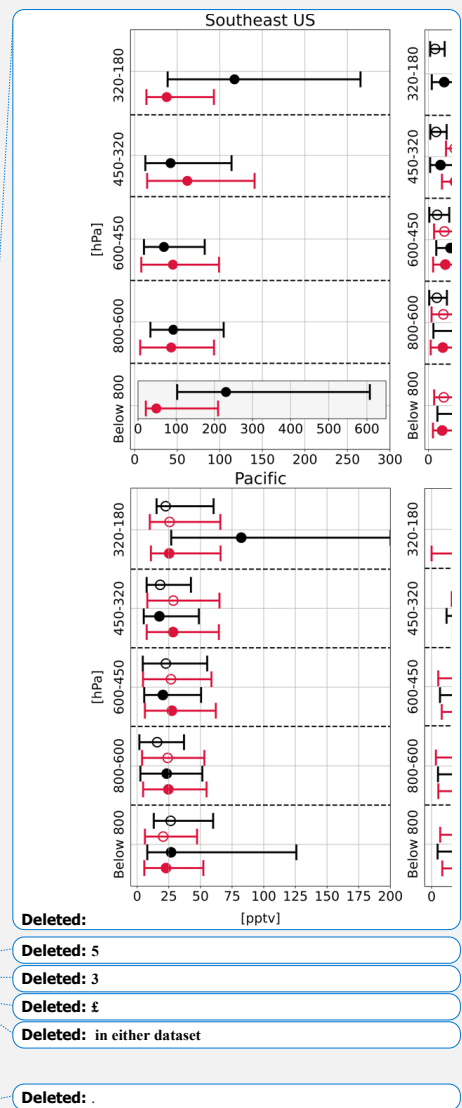
Large differences between DC-8 and cloud-sliced NO₂ occur in the boundary layer and the top tropospheric layer. In these layers, there are few coincident data points (Fig. 5). Most DC-8 data in these 2 layers are over land influenced by ground-based

sources like intense biomass burning in the boundary layer (Alvarado et al., 2010; Bian et al., 2013) and lightning and convective uplift of surface pollution in the upper troposphere, whereas most cloud-sliced NO_2 in these 2 layers are over the ocean (Fig. 5). The cluster of points in the boundary layer over New England in the northeast US in Fig. 5 have similar coverage from both datasets. These are on median 30 pptv (IQR: 20-50 pptv) for DC-8 and 25 pptv (IQR: 20-30 pptv) for cloud-sliced NO_2. New England is not included in our comparison in Fig. 6 and 7, as sampling over this location is limited to JJA during INTEX-A.
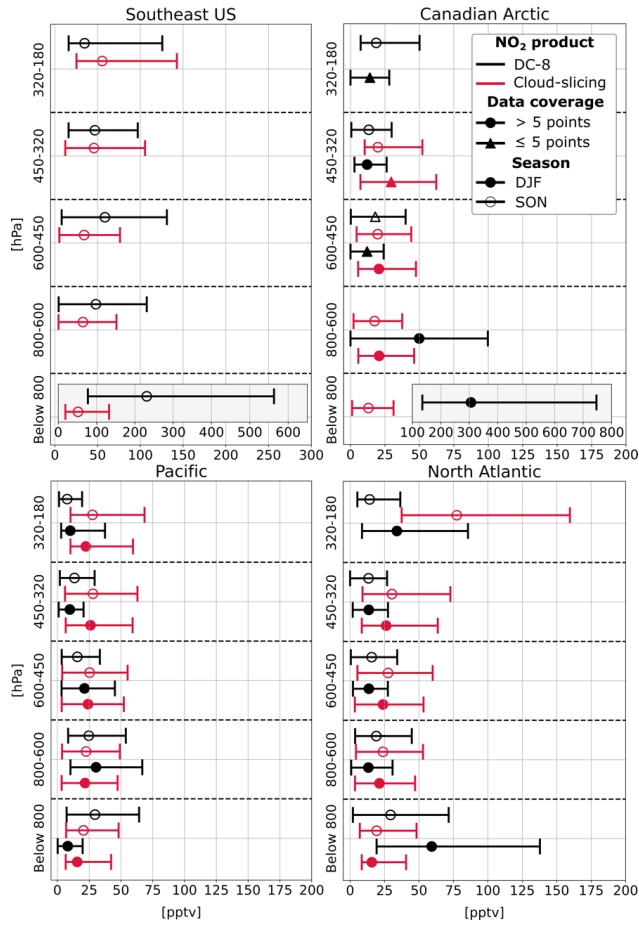
440 **Figure 7: As in Fig. 6, but for SON (open symbols) and DJF (filled symbols).**

3.3 Comparison of cloud-sliced vertical profiles to synthetic GEOS-Chem profiles

Fig. 8 shows the percent difference between multiyear mean GEOS-Chem and cloud-sliced NO_2 for June-August and

December-February obtained after regridding the cloud-sliced NO_2 to the GEOS-Chem $2° \times 2.5°$ grid. Multiyear means in

445 both datasets are compared to minimise influence of interannual variability quantified in Section 3.1. In general, GEOS-Chem

NO_2 is 30-80% (10-25 pptv) less than cloud-sliced NO_2 in remote locations. Specifically, the Southern Ocean in all layers

retrieved, South America throughout the free troposphere, and all grid cells except those over Africa in the upper troposphere.

Similar spatial patterns and magnitudes of discrepancies to those plotted in Fig. 8 occur in March-May and September-

November.

450
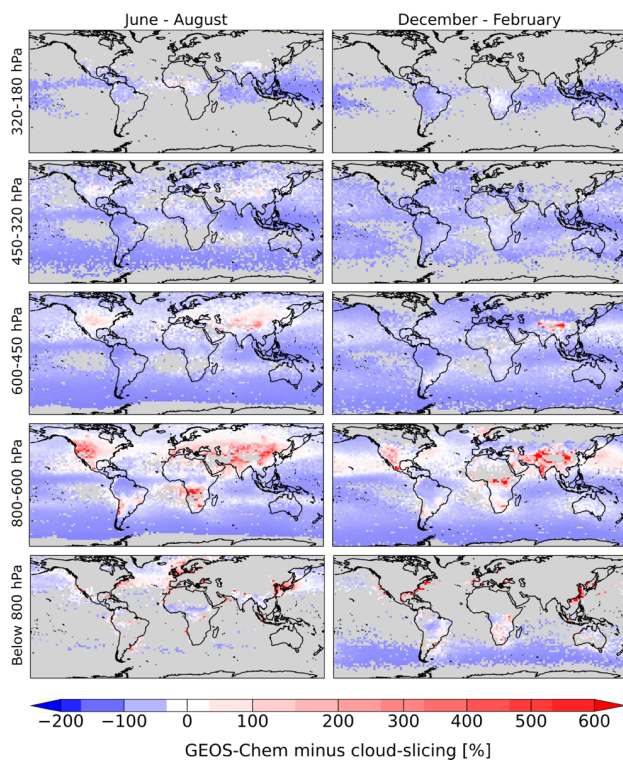
455

Figure 8: Percent difference between cloud-sliced and GEOS-Chem vertical profiles of tropospheric NO₂. Maps are at 2° × 2.5°. Blue (red) indicates the model is less (more) than the cloud-sliced NO₂. Percent difference is calculated as ((GEOS-Chem minus cloud-sliced)/cloud-sliced) for all cloud-sliced 1° × 1° grid squares filled in each year sampled.

460

Inclusion of nitrate photolysis in GEOS-Chem decreases the model underestimate in NO₂ over remote regions from 40-80 pptv to on average ~15 pptv in the mid-troposphere. A relatively large model underestimate of 25-40 pptv over oceans may be due to uncertainties in the enhancement factor used to parameterise nitrate photolysis (Section 2.3) (Shah et al., 2023). PPN photolysis is most effective at increasing NO₂ in the 2 layers in the upper troposphere where it is abundant and thermally stable, so photolysis dominates its conversion to NO₂. In JJA, for example, PPN photolysis contributes ~65 pptv NO₂ over the northern midlatitudes and isolated enhancements of 50-60 pptv over southeast Asia and extending from Mozambique to Madagascar. As a result of PPN photolysis, the discrepancy between the model and cloud-sliced upper tropospheric NO₂ is relatively small

465

(10-30 pptv) over the terrestrial northern midlatitudes. The model exceeds the cloud-sliced data by 20-50 pptv over the northern midlatitudes at 600-450 hPa during the summer lightning season north of 35°N. These are the latitudes at which lightning NO_x production rates in GEOS-Chem almost double from 260 moles per flash (mol fl^{-1}) to the south to 500 mol fl^{-1} to the north (Murray et al., 2012). The effect of this on NO_2 is also evident at 450-320 hPa, though the spatial extent and dataset differences are smaller in this layer. 500 mol fl^{-1} prescribed to northern midlatitude lightning far exceeds observationally constrained global mean estimates of ~280 mol fl^{-1} (Marais et al., 2018) and regional mean estimates of 180 mol fl^{-1} for the northern midlatitudes (Bucsela et al., 2019) and 230-360 mol fl^{-1} for the US and western Atlantic (Allen et al., 2021).

The largest differences between the two datasets occur in the boundary layer along coastlines in North America, Europe and China influenced by anthropogenic pollution. This may in part be due to the different years targeted. COVID lockdowns influenced surface emissions of traffic NO_x in the cloud-sliced data and anthropogenic NO_x emissions are steadily declining over North America, Europe and China as a result of air quality regulation (Zhao et al., 2013; Lloret and Valiela, 2016; Clappier et al., 2021). Both COVID lockdowns and emissions reductions policies would contribute to a model overestimate in NO_2. GEOS-Chem also exceeds cloud-sliced NO_2 at multiple locations in the 800-600 hPa layer. These include southern Africa in JJA and northern Africa in DJF coincident with the dry burning season of these regions, central Asia in all seasons where there are large sources of anthropogenic pollution. The apparent model overestimate over western US at 600-800 hPa occurs in all seasons and may result from a combination of factors. The TROPOMI sampling period includes the high-fire year (2020) (Albores et al., 2023) and the model does not, affecting the comparison in seasons coincident with the fire season (JJA, SON). The number of cloud-sliced data points are also relatively few over this region of subsidence. It is difficult to diagnose discrepancies in the tropical terrestrial boundary layer, as anthropogenic emissions inventories are prone to misrepresenting sources unique to the tropics (Duncan et al., 2003; Marais and Wiedinmyer, 2016; Vohra et al., 2022) and there are no suitable independent in-situ measurements to validate the differencing approach we use to derive NO_2.

4 Conclusions

Global vertical profiles of tropospheric NO_2 were obtained for five discrete layers (180-320 hPa, 320-450 hPa, 450-600 hPa, 600-800 hPa, and below 800 hPa) by cloud-slicing TROPOMI total columns of NO_2 above optically thick clouds. These we assessed against directly measured and calculated (photostationary steady-state) NASA DC-8 aircraft NO_2 measurements from 2004 to 2018. We then applied our cloud-sliced NO_2 to evaluate contemporary understanding of climatological tropospheric NO_x as simulated by GEOS-Chem. We found that coverage from cloud-slicing is greatest in the mid-troposphere (60-70%) where there is an abundance of optically thick clouds and least (8% coverage, mostly in the tropics) in the upper troposphere. Cloud-sliced NO_2 ranges from < 35 pptv throughout the troposphere over remote marine regions, to 20-60 pptv in the free troposphere over continents, to 160-380 pptv in the boundary layer over source regions in the US, Europe and Asia. Free tropospheric NO_2 exhibits very little interannual variability, ranging from ~10 pptv over oceans to ~25 pptv over land.

We determined from comparison of cloud-sliced NO_2 to NASA DC-8 aircraft observations that cloud-sliced NO_2 differs from DC-8 NO_2 by just 5-15 pptv when sampling in both datasets is abundant and consistent. It was not feasible to assess cloud-sliced NO_2 in the boundary layer and in the highest cloud-sliced layer, due to a lack of sufficient coincident data in the tropics.

505 The GEOS-Chem model that represents contemporary understanding of tropospheric NO_x simulates NO_2 that is typically 10-40 pptv less than cloud-sliced NO_2 in the remote upper troposphere and over the remote oceans. This is a substantial improvement on the > 40 pptv model underestimate before accounting for NO_x recycling in the upper troposphere via PPN photolysis and in the middle and lower troposphere via aerosol nitrate photolysis. Differences are greater over source regions influenced by lightning and open burning of biomass and with evolving anthropogenic emissions due to rapid development,

510 policies and events like lockdowns in response to the COVID-19 pandemic. A model high bias of 50 pptv over the northern hemisphere mid-troposphere in June-August points to an issue with the model lightning NO_x production rates that are almost double production rates everywhere else.

Limited coincident reliable observations to validate cloud-sliced NO_2 remains a challenge, but as we demonstrate cloud-sliced

515 NO_2 hold value for assessing air quality, chemical transport, and Earth System models to identify differences that warrant further investigation, especially given reliance on these models to understand complex tropospheric chemistry, inform policies, and retrieve trace gas abundances from satellites. Geostationary instruments will further enhance the utility of cloud-sliced NO_2 datasets to also investigate daytime variability in vertical profiles of tropospheric NO_x.

520

525

530

Deleted: 10

Data Availability. The multiyear seasonal mean NO$_2$ from cloud-slicing TROPOMI and from simulating the GEOS-Chem model are publicly available from the UCL Data Repository (https://doi.org/10.5522/04/25782336).

535

Author contributions. Study concept by EAM and RPH. RPH led the writing and analysis, simulated GEOS-Chem and cloud-sliced TROPOMI NO$_2$ with supervision from EAM. NW provided the NASA DC-8 python processing code. RGR updated the GEOS-Chem model to include PPN photolysis. VS updated the GEOS-Chem model to include particulate nitrate photolysis. All authors reviewed and edited the manuscript.

540

Competing interests. The authors declare that they have no conflict of interest.

Acknowledgements. This research has been supported by the European Research Council under the European Union's Horizon 2020 research and innovation programme (through a Starting Grant awarded to Eloise A. Marais, UpTrop [grant no. 851854]).

545 We are grateful to NASA DC-8 aircraft campaign teams for access to observations, specifically the NO$_2$ measurement PIs: Ronald Cohen (INTEX-A and INTEX-B), Andrew Weinheimer (ARCTAS), Thomas B. Ryerson (SEAC^{4}RS), and Chelsea Thompson (ATom).

References

550

Albores, I. S., Buchholz, R. R., Ortega, I., Emmons, L. K., Hannigan, J. W., Lacey, F., Pfister, G., Tang, W., and Worden, H. M.: Continental-scale Atmospheric Impacts of the 2020 Western U.S. Wildfires, Atmos. Environ., 294, 119436, https://doi.org/10.1016/j.atmosenv.2022.119436, 2023.

Allen, D. J., Pickering, K. E., Lamsal, L., Mach, D. M., Quick, M. G., Lapierre, J., Janz, S., Koshak, W., Kowalewski, M., and
555 Blakeslee, R.: Observations of Lightning NO_x Production From GOES-R Post Launch Test Field Campaign Flights, J. Geophys. Res. Atmospheres, 126, e2020JD033769, https://doi.org/10.1029/2020JD033769, 2021.

Alvarado, M. J., Logan, J. A., Mao, J., Apel, E., Riemer, D., Blake, D., Cohen, R. C., Min, K.-E., Perring, A. E., Browne, E. C., Wooldridge, P. J., Diskin, G. S., Sachse, G. W., Fuelberg, H., Sessions, W. R., Harrigan, D. L., Huey, G., Liao, J., Case-Hanks, A., Jimenez, J. L., Cubison, M. J., Vay, S. A., Weinheimer, A. J., Knapp, D. J., Montzka, D. D., Flocke, F. M., Pollack,
560 I. B., Wennberg, P. O., Kurten, A., Crounse, J., Clair, J. M. St., Wisthaler, A., Mikoviny, T., Yantosca, R. M., Carouge, C. C., and Le Sager, P.: Nitrogen oxides and PAN in plumes from boreal fires during ARCTAS-B and their impact on ozone: an integrated analysis of aircraft and satellite observations, Atmospheric Chem. Phys., 10, 9739–9760, https://doi.org/10.5194/acp-10-9739-2010, 2010.

Andersen, S. T., Carpenter, L. J., Reed, C., Lee, J. D., Chance, R., Sherwen, T., Vaughan, A. R., Stewart, J., Edwards, P. M.,
565 Bloss, W. J., Sommariva, R., Crilley, L. R., Nott, G. J., Neves, L., Read, K., Heard, D. E., Seakins, P. W., Whalley, L. K., Boustead, G. A., Fleming, L. T., Stone, D., and Fomba, K. W.: Extensive field evidence for the release of HONO from the photolysis of nitrate aerosols, Sci. Adv., 9, https://doi.org/10.1126/sciadv.add6266, 2023.

Andreae, M. O., Artaxo, P., Fischer, H., Freitas, S. R., Grégoire, J.-M., Hansel, A., Hoor, P., Kormann, R., Krejci, R., Lange, L., Lelieveld, J., Lindinger, W., Longo, K., Peters, W., De Reus, M., Scheeren, B., Silva Dias, M. A. F., Ström, J., Van
570 Velthoven, P. F. J., and Williams, J.: Transport of biomass burning smoke to the upper troposphere by deep convection in the equatorial region, Geophys. Res. Lett., 28, 951–954, https://doi.org/10.1029/2000GL012391, 2001.

ARCTAS Science Team: Arctic Research of the Composition of the Troposphere from Aircraft and Satellites (ARCTAS) NASA Airborne Mission Overview, https://doi.org/10.5067/SUBORBITAL/ARCTAS2008/DATA001, 2011.

Atkinson, R.: Atmospheric chemistry of VOCs and NO_x, Atmos. Environ., 34, 2063–2101, https://doi.org/10.1016/S1352-
575 2310(99)00460-4, 2000.

ATom Science Team: Atmospheric Tomography Mission (ATom): Merged Atmospheric Chemistry, Trace Gases, and Aerosols, Version 2, https://doi.org/10.3334/ORNLDAAC/1925, 2021.

Barth, M. C., Cantrell, C. A., Brune, W. H., Rutledge, S. A., Crawford, J. H., Huntrieser, H., Carey, L. D., MacGorman, D., Weisman, M., Pickering, K. E., Bruning, E., Anderson, B., Apel, E., Biggerstaff, M., Campos, T., Campuzano-Jost, P., Cohen,
580 R., Crounse, J., Day, D. A., Diskin, G., Flocke, F., Fried, A., Garland, C., Heikes, B., Honomichl, S., Hornbrook, R., Huey, L. G., Jimenez, J. L., Lang, T., Lichtenstern, M., Mikoviny, T., Nault, B., O'Sullivan, D., Pan, L. L., Peischl, J., Pollack, I., Richter, D., Riemer, D., Ryerson, T., Schlager, H., St. Clair, J., Walega, J., Weibring, P., Weinheimer, A., Wennberg, P., Wisthaler, A., Wooldridge, P. J., and Ziegler, C.: The Deep Convective Clouds and Chemistry (DC3) Field Campaign, Bull. Am. Meteorol. Soc., 96, 1281–1309, https://doi.org/10.1175/BAMS-D-13-00290.1, 2015.

585 Beirle, S., Borger, C., Dörner, S., Li, A., Hu, Z., Liu, F., Wang, Y., and Wagner, T.: Pinpointing nitrogen oxide emissions from space, Sci. Adv., 5, eaax9800, https://doi.org/10.1126/sciadv.aax9800, 2019.

Belmonte Rivas, M., Veefkind, P., Eskes, H., and Levelt, P.: OMI tropospheric NO_2 profiles from cloud slicing: constraints on surface emissions, convective transport and lightning NO_x, Atmospheric Chem. Phys. Discuss., 15, 8017–8072, https://doi.org/10.5194/acpd-15-8017-2015, 2015.

590 Bertram, T. H., Perring, A. E., Wooldridge, P. J., Crounse, J. D., Kwan, A. J., Wennberg, P. O., Scheuer, E., Dibb, J., Avery, M., Sachse, G., Vay, S. A., Crawford, J. H., McNaughton, C. S., Clarke, A., Pickering, K. E., Fuelberg, H., Huey, G., Blake, D. R., Singh, H. B., Hall, S. R., Shetter, R. E., Fried, A., Heikes, B. G., and Cohen, R. C.: Direct Measurements of the Convective Recycling of the Upper Troposphere, Science, 315, 816–820, https://doi.org/10.1126/science.1134548, 2007.

Bian, H., Colarco, P. R., Chin, M., Chen, G., Rodriguez, J. M., Liang, Q., Blake, D., Chu, D. A., Da Silva, A., Darmenov, A. 595 S., Diskin, G., Fuelberg, H. E., Huey, G., Kondo, Y., Nielsen, J. E., Pan, X., and Wisthaler, A.: Source attributions of pollution to the Western Arctic during the NASA ARCTAS field campaign, Atmospheric Chem. Phys., 13, 4707–4721, https://doi.org/10.5194/acp-13-4707-2013, 2013.

Bloss, W. J., Evans, M. J., Lee, J. D., Sommariva, R., Heard, D. E., and Pilling, M. J.: The oxidative capacity of the troposphere: Coupling of field measurements of OH and a global chemistry transport model, Faraday Discuss., 130, 425, 600 https://doi.org/10.1039/b419090d, 2005.

Boersma, K. F., Eskes, H. J., and Brinksma, E. J.: Error analysis for tropospheric NO_2 retrieval from space, J. Geophys. Res. Atmospheres, 109, https://doi.org/10.1029/2003JD003962, 2004.

Bradshaw, J., Davis, D., Grodzinsky, G., Smyth, S., Newell, R., Sandholm, S., and Liu, S.: Observed distributions of nitrogen oxides in the remote free troposphere from the Nasa Global Tropospheric Experiment Programs, Rev. Geophys., 38, 61–116, 605 https://doi.org/10.1029/1999RG900015, 2000.

Brenninkmeijer, C. A. M., Crutzen, P. J., Fischer, H., Güsten, H., Hans, W., Heinrich, G., Heintzenberg, J., Hermann, M., Immelmann, T., Kersting, D., Maiss, M., Nolle, M., Pitscheider, A., Pohlkamp, H., Scharffe, D., Specht, K., and Wiedensohler, A.: CARIBIC—Civil Aircraft for Global Measurement of Trace Gases and Aerosols in the Tropopause Region, J. Atmospheric Ocean. Technol., 16, 1373–1383, https://doi.org/10.1175/1520-0426(1999)016<1373:CCAFGM>2.0.CO;2, 1999.

610 Browne, E. C., Perring, A. E., Wooldridge, P. J., Apel, E., Hall, S. R., Huey, L. G., Mao, J., Spencer, K. M., Clair, J. M. St., Weinheimer, A. J., Wisthaler, A., and Cohen, R. C.: Global and regional effects of the photochemistry of $CH_3O_2NO_2$ evidence from ARCTAS, Atmospheric Chem. Phys., 11, 4209–4219, https://doi.org/10.5194/acp-11-4209-2011, 2011.

Bucsela, E. J., Pickering, K. E., Allen, D. J., Holzworth, R. H., and Krotkov, N. A.: Midlatitude Lightning NO $_x$ Production Efficiency Inferred From OMI and WWLLN Data, J. Geophys. Res. Atmospheres, 124, 13475–13497, 615 https://doi.org/10.1029/2019JD030561, 2019.

Burkholder, J. B., Sander, S. P., Abbatt, J. P. D., Barker, J. R., Cappa, C., Crounse, J. D., Dibble, T. S., Huie, R. E., Kolb, C. E., Kurylo, M. J., Orkin, V. L., Percival, C. J., Wilmouth, D. M., and Wine, P. H.: Chemical Kinetics and Photochemical Data for Use in Atmospheric Studies, Evaluation No. 19, 2020.

Castellanos, P., Boersma, K. F., and Van Der Werf, G. R.: Satellite observations indicate substantial spatiotemporal variability 620 in biomass burning NO_x emission factors for South America, Atmospheric Chem. Phys., 14, 3929–3943, https://doi.org/10.5194/acp-14-3929-2014, 2014.

Chatfield, R. B.: Anomalous HNO_3 /NO_x ratio of remote tropospheric air: Conversion of nitric acid to formic acid and NO_x?, Geophys. Res. Lett., 21, 2705–2708, https://doi.org/10.1029/94GL02659, 1994.

Chen, Y., Morton, D. C., Jin, Y., Collatz, G. J., Kasibhatla, P. S., Van Der Werf, G. R., DeFries, R. S., and Randerson, J. T.: Long-term trends and interannual variability of forest, savanna and agricultural fires in South America, Carbon Manag., 4, 617–638, https://doi.org/10.4155/cmt.13.61, 2013.

Choi, S., Joiner, J., Choi, Y., Duncan, B. N., Vasilkov, A., Krotkov, N., and Bucsela, E.: First estimates of global free-tropospheric NO_2 abundances derived using a cloud-slicing technique applied to satellite observations from the Aura Ozone Monitoring Instrument (OMI), Atmospheric Chem. Phys., 14, 10565–10588, https://doi.org/10.5194/acp-14-10565-2014, 2014.

Christian, H. J., Blakeslee, R. J., Boccippio, D. J., Boeck, W. L., Buechler, D. E., Driscoll, K. T., Goodman, S. J., Hall, J. M., Koshak, W. J., Mach, D. M., and Stewart, M. F.: Global frequency and distribution of lightning as observed from space by the Optical Transient Detector, J. Geophys. Res. Atmospheres, 108, https://doi.org/10.1029/2002JD002347, 2003.

Clappier, A., Thunis, P., Beekmann, M., Putaud, J. P., and De Meij, A.: Impact of SO_x, NO_x and NH_3 emission reductions on $PM_{2.5}$ concentrations across Europe: Hints for future measure development, Environ. Int., 156, 106699, https://doi.org/10.1016/j.envint.2021.106699, 2021.

Crawford, J., Davis, D., Chen, G., Bradshaw, J., Sandholm, S., Gregory, G., Sachse, G., Anderson, B., Collins, J., Blake, D., Singh, H., Heikes, B., Talbot, R., and Rodriguez, J.: Photostationary state analysis of the NO_2-NO system based on airborne observations from the western and central North Pacific, J. Geophys. Res. Atmospheres, 101, 2053–2072, https://doi.org/10.1029/95JD02201, 1996.

Crutzen, P. J. and Andreae, M. O.: Biomass Burning in the Tropics: Impact on Atmospheric Chemistry and Biogeochemical Cycles, Science, 250, 1669–1678, https://doi.org/10.1126/science.250.4988.1669, 1990.

Davis, D. D., Chen, G., Chameides, W., Bradshaw, J., Sandholm, S., Rodgers, M., Schendal, J., Madronich, S., Sachse, G., Gregory, G., Anderson, B., Barrick, J., Shipham, M., Collins, J., Wade, L., and Blake, D.: A photostationary state analysis of the NO_2-NO system based on airborne observations from the subtropical/tropical North and South Atlantic, J. Geophys. Res., 98, 23501, https://doi.org/10.1029/93JD02412, 1993.

Di Carlo, P., Aruffo, E., Busilacchio, M., Giammaria, F., Dari-Salisburgo, C., Biancofiore, F., Visconti, G., Lee, J., Moller, S., Reeves, C. E., Bauguitte, S., Forster, G., Jones, R. L., and Ouyang, B.: Aircraft based four-channel thermal dissociation laser induced fluorescence instrument for simultaneous measurements of NO_2, total peroxy nitrate, total alkyl nitrate, and HNO_3, Atmospheric Meas. Tech., 6, 971–980, https://doi.org/10.5194/amt-6-971-2013, 2013.

Dickerson, R. R., Stedman, D. H., and Delany, A. C.: Direct measurements of ozone and nitrogen dioxide photolysis rates in the troposphere, J. Geophys. Res. Oceans, 87, 4933–4946, https://doi.org/10.1029/JC087iC07p04933, 1982.

Dignon, J.: NO_x and SO_x emissions from fossil fuels: A global distribution, Atmospheric Environ. Part Gen. Top., 26, 1157–1163, https://doi.org/10.1016/0960-1686(92)90047-O, 1992.

Duncan, B. N., Martin, R. V., Staudt, A. C., Yevich, R., and Logan, J. A.: Interannual and seasonal variability of biomass burning emissions constrained by satellite observations, J. Geophys. Res., 108, 4100, https://doi.org/10.1029/2002JD002378, 2003.

Ehhalt, D. H., Rohrer, F., and Wahner, A.: Sources and distribution of NO_x in the upper troposphere at northern mid-latitudes, J. Geophys. Res., 97, 3725, https://doi.org/10.1029/91JD03081, 1992.

660   Emmons, L. K., Hauglustaine, D. A., Müller, J., Carroll, M. A., Brasseur, G. P., Brunner, D., Staehelin, J., Thouret, V., and Marenco, A.: Data composites of airborne observations of tropospheric ozone and its precursors, J. Geophys. Res. Atmospheres, 105, 20497–20538, https://doi.org/10.1029/2000JD900232, 2000.

Eskes, H. J. and Eichmann, K.-U.: S5P Mission Performance Centre Nitrogen Dioxide [L2__NO2___] Readme, 2023.

Fuelberg, H. E., Hannan, J. R., Van Velthoven, P. F. J., Browell, E. V., Bieberbach, G., Knabb, R. D., Gregory, G. L., Pickering,
665   K. E., and Selkirk, H. B.: A meteorological overview of the Subsonic Assessment Ozone and Nitrogen Oxide Experiment (SONEX) period, J. Geophys. Res. Atmospheres, 105, 3633–3651, https://doi.org/10.1029/1999JD900917, 2000.

Ghude, S. D., Kulkarni, S. H., Jena, C., Pfister, G. G., Beig, G., Fadnavis, S., and Van Der A, R. J.: Application of satellite observations for identifying regions of dominant sources of nitrogen oxides over the Indian Subcontinent, J. Geophys. Res. Atmospheres, 118, 1075–1089, https://doi.org/10.1029/2012JD017811, 2013.

670   Giglio, L., Randerson, J. T., Van Der Werf, G. R., Kasibhatla, P. S., Collatz, G. J., Morton, D. C., and DeFries, R. S.: Assessing variability and long-term trends in burned area by merging multiple satellite fire products, Biogeosciences, 7, 1171–1186, https://doi.org/10.5194/bg-7-1171-2010, 2010.

Grewe, V., Brunner, D., Dameris, M., Grenfell, J. L., Hein, R., Shindell, D., and Staehelin, J.: Origin and variability of upper tropospheric nitrogen oxides and ozone at northern mid-latitudes, Atmos. Environ., 35, 3421–3433,
675   https://doi.org/10.1016/S1352-2310(01)00134-0, 2001.

Guo, H., Flynn, C. M., Prather, M. J., Strode, S. A., Steenrod, S. D., Emmons, L., Lacey, F., Lamarque, J.-F., Fiore, A. M., Correa, G., Murray, L. T., Wolfe, G. M., St. Clair, J. M., Kim, M., Crounse, J., Diskin, G., DiGangi, J., Daube, B. C., Commane, R., McKain, K., Peischl, J., Ryerson, T. B., Thompson, C., Hanisco, T. F., Blake, D., Blake, N. J., Apel, E. C., Hornbrook, R. S., Elkins, J. W., Hintsa, E. J., Moore, F. L., and Wofsy, S. C.: Heterogeneity and chemical reactivity of the remote troposphere
680   defined by aircraft measurements, Atmospheric Chem. Phys., 23, 99–117, https://doi.org/10.5194/acp-23-99-2023, 2023.

Harwood, M. H., Roberts, J. M., Frost, G. J., Ravishankara, A. R., and Burkholder, J. B.: Photochemical Studies of $CH_3C(O)OONO_2$ (PAN) and $CH_3CH_2C(O)OONO_2$ (PPN): NO_3 Quantum Yields, J. Phys. Chem. A, 107, 1148–1154, https://doi.org/10.1021/jp0264230, 2003.

Hudman, R. C., Jacob, D. J., Turquety, S., Leibensperger, E. M., Murray, L. T., Wu, S., Gilliland, A. B., Avery, M., Bertram,
685   T. H., Brune, W., Cohen, R. C., Dibb, J. E., Flocke, F. M., Fried, A., Holloway, J., Neuman, J. A., Orville, R., Perring, A., Ren, X., Sachse, G. W., Singh, H. B., Swanson, A., and Wooldridge, P. J.: Surface and lightning sources of nitrogen oxides over the United States: Magnitudes, chemical evolution, and outflow, J. Geophys. Res. Atmospheres, 112, 2006JD007912, https://doi.org/10.1029/2006JD007912, 2007.

Jacob, D. J., Crawford, J. H., Maring, H., Clarke, A. D., Dibb, J. E., Emmons, L. K., Ferrare, R. A., Hostetler, C. A., Russell,
690   P. B., Singh, H. B., Thompson, A. M., Shaw, G. E., McCauley, E., Pederson, J. R., and Fisher, J. A.: The Arctic Research of the Composition of the Troposphere from Aircraft and Satellites (ARCTAS) mission: design, execution, and first results, Atmospheric Chem. Phys., 10, 5191–5212, https://doi.org/10.5194/acp-10-5191-2010, 2010.

Jaeglé, L., Jacob, D. J., Wang, Y., Weinheimer, A. J., Ridley, B. A., Campos, T. L., Sachse, G. W., and Hagen, D. E.: Sources and chemistry of NO_x in the upper troposphere over the United States, Geophys. Res. Lett., 25, 1705–1708,
695   https://doi.org/10.1029/97GL03591, 1998.

Jain, A. K., Tao, Z., Yang, X., and Gillespie, C.: Estimates of global biomass burning emissions for reactive greenhouse gases (CO, NMHCs, and NO_x) and CO_2, J. Geophys. Res., 111, D06304, https://doi.org/10.1029/2005JD006237, 2006.

Jin, X., Zhu, Q., and Cohen, R. C.: Direct estimates of biomass burning NO_x emissions and lifetimes using daily observations from TROPOMI, Atmospheric Chem. Phys., 21, 15569–15587, https://doi.org/10.5194/acp-21-15569-2021, 2021.

700 Kang, Y., Tang, G., Li, Q., Liu, B., Cao, J., Hu, Q., and Wang, Y.: Evaluation and Evolution of MAX-DOAS-observed Vertical NO_2 Profiles in Urban Beijing, Adv. Atmospheric Sci., 38, 1188–1196, https://doi.org/10.1007/s00376-021-0370-1, 2021.

Karl, T. G., Christian, T. J., Yokelson, R. J., Artaxo, P., Hao, W. M., and Guenther, A.: The Tropical Forest and Fire Emissions Experiment: method evaluation of volatile organic compound emissions measured by PTR-MS, FTIR, and GC from tropical biomass burning, Atmospheric Chem. Phys., 7, 5883–5897, https://doi.org/10.5194/acp-7-5883-2007, 2007.

705 Kasibhatla, P., Sherwen, T., Evans, M. J., Carpenter, L. J., Reed, C., Alexander, B., Chen, Q., Sulprizio, M. P., Lee, J. D., Read, K. A., Bloss, W., Crilley, L. R., Keene, W. C., Pszenny, A. A. P., and Hodzic, A.: Global impact of nitrate photolysis in sea-salt aerosol on NO_x, OH, and O_3 in the marine boundary layer, Atmospheric Chem. Phys., 18, 11185–11203, https://doi.org/10.5194/acp-18-11185-2018, 2018.

Kawakami, S., Kondo, Y., Koike, M., Nakajima, H., Gregory, G. L., Sachse, G. W., Newell, R. E., Browell, E. V., Blake, D. 710 R., Rodriguez, J. M., and Merrill, J. T.: Impact of lightning and convection on reactive nitrogen in the tropical free troposphere, J. Geophys. Res. Atmospheres, 102, 28367–28384, https://doi.org/10.1029/97JD02073, 1997.

Keita, S., Liousse, C., Assamoi, E.-M., Doumbia, T., N'Datchoh, E. T., Gnamien, S., Elguindi, N., Granier, C., and Yoboué, V.: African anthropogenic emissions inventory for gases and particles from 1990 to 2015, Earth Syst. Sci. Data, 13, 3691–3705, https://doi.org/10.5194/essd-13-3691-2021, 2021.

715 Kenagy, H. S., Sparks, T. L., Ebben, C. J., Wooldrige, P. J., Lopez-Hilfiker, F. D., Lee, B. H., Thornton, J. A., McDuffie, E. E., Fibiger, D. L., Brown, S. S., Montzka, D. D., Weinheimer, A. J., Schroder, J. C., Campuzano-Jost, P., Day, D. A., Jimenez, J. L., Dibb, J. E., Campos, T., Shah, V., Jaeglé, L., and Cohen, R. C.: NO_x Lifetime and NO_y Partitioning During WINTER, J. Geophys. Res. Atmospheres, 123, 9813–9827, https://doi.org/10.1029/2018JD028736, 2018.

Kotamarthi, V. R., Gaffney, J. S., Marley, N. A., and Doskey, P. V.: Heterogeneous NO_x chemistry in the polluted PBL, 720 Atmos. Environ., 35, 4489–4498, https://doi.org/10.1016/S1352-2310(01)00221-7, 2001.

Liu, S., Valks, P., Pinardi, G., Xu, J., Chan, K. L., Argyrouli, A., Lutz, R., Beirle, S., Khorsandi, E., Baier, F., Huijnen, V., Bais, A., Donner, S., Dörner, S., Gratsea, M., Hendrick, F., Karagkiozidis, D., Lange, K., Piters, A. J. M., Remmers, J., Richter, A., Van Roozendael, M., Wagner, T., Wenig, M., and Loyola, D. G.: An improved TROPOMI tropospheric NO_2 research product over Europe, Atmospheric Meas. Tech., 14, 7297–7327, https://doi.org/10.5194/amt-14-7297-2021, 2021.

725 Lloret, J. and Valiela, I.: Unprecedented decrease in deposition of nitrogen oxides over North America: the relative effects of emission controls and prevailing air-mass trajectories, Biogeochemistry, 129, 165–180, https://doi.org/10.1007/s10533-016-0225-5, 2016.

Loyola, D. G., Gimeno García, S., Lutz, R., Argyrouli, A., Romahn, F., Spurr, R. J. D., Pedergnana, M., Doicu, A., Molina García, V., and Schüssler, O.: The operational cloud retrieval algorithms from TROPOMI on board Sentinel-5 Precursor, 730 Atmospheric Meas. Tech., 11, 409–427, https://doi.org/10.5194/amt-11-409-2018, 2018.

Lu, G., Marais, E. A., Vohra, K., Horner, R. P., Zhang, D., Martin, R. V., and Guttikunda, S. K.: Near-Automated Estimate of City Nitrogen Oxides Emissions Applied to South and Southeast Asia, https://doi.org/10.22541/essoar.171033213.36792308/v1, 13 March 2024.

Marais, E. A. and Wiedinmyer, C.: Air Quality Impact of Diffuse and Inefficient Combustion Emissions in Africa (DICE-735 Africa), Environ. Sci. Technol., 50, 10739–10745, https://doi.org/10.1021/acs.est.6b02602, 2016.

Marais, E. A., Jacob, D. J., Jimenez, J. L., Campuzano-Jost, P., Day, D. A., Hu, W., Krechmer, J., Zhu, L., Kim, P. S., Miller, C. C., Fisher, J. A., Travis, K., Yu, K., Hanisco, T. F., Wolfe, G. M., Arkinson, H. L., Pye, H. O. T., Froyd, K. D., Liao, J., and McNeill, V. F.: Aqueous-phase mechanism for secondary organic aerosol formation from isoprene: application to the southeast United States and co-benefit of SO_2 emission controls, Atmospheric Chem. Phys., 16, 1603–1618, https://doi.org/10.5194/acp-16-1603-2016, 2016.

Marais, E. A., Jacob, D. J., Choi, S., Joiner, J., Belmonte-Rivas, M., Cohen, R. C., Beirle, S., Murray, L. T., Schiferl, L. D., Shah, V., and Jaeglé, L.: Nitrogen oxides in the global upper troposphere: interpreting cloud-sliced NO_2 observations from the OMI satellite instrument, Atmospheric Chem. Phys., 18, 17017–17027, https://doi.org/10.5194/acp-18-17017-2018, 2018.

Marais, E. A., Roberts, J. F., Ryan, R. G., Eskes, H., Boersma, K. F., Choi, S., Joiner, J., Abuhassan, N., Redondas, A., Grutter, M., Cede, A., Gomez, L., and Navarro-Comas, M.: New observations of NO_2 in the upper troposphere from TROPOMI, Atmospheric Meas. Tech., 14, 2389–2408, https://doi.org/10.5194/amt-14-2389-2021, 2021.

McDuffie, E. E., Smith, S. J., O'Rourke, P., Tibrewal, K., Venkataraman, C., Marais, E. A., Zheng, B., Crippa, M., Brauer, M., and Martin, R. V.: A global anthropogenic emission inventory of atmospheric pollutants from sector- and fuel-specific sources (1970–2017): an application of the Community Emissions Data System (CEDS), Earth Syst. Sci. Data, 12, 3413–3442, https://doi.org/10.5194/essd-12-3413-2020, 2020.

Meng, J., Martin, R. V., Ginoux, P., Hammer, M., Sulprizio, M. P., Ridley, D. A., and Van Donkelaar, A.: Grid-independent high-resolution dust emissions (v1.0) for chemical transport models: application to GEOS-Chem (12.5.0), Geosci. Model Dev., 14, 4249–4260, https://doi.org/10.5194/gmd-14-4249-2021, 2021.

Moxim, W. J., Levy, H., and Kasibhatla, P. S.: Simulated global tropospheric PAN: Its transport and impact on NO_x, J. Geophys. Res. Atmospheres, 101, 12621–12638, https://doi.org/10.1029/96JD00338, 1996.

Murphy, J. G., Thornton, J. A., Wooldridge, P. J., Day, D. A., Rosen, R. S., Cantrell, C., Shetter, R. E., Lefer, B., and Cohen, R. C.: Measurements of the sum of HO_2NO_2 and $CH_3O_2NO_2$ in the remote troposphere, Atmospheric Chem. Phys., 4, 377–384, https://doi.org/10.5194/acp-4-377-2004, 2004.

Murray, L. T., Jacob, D. J., Logan, J. A., Hudman, R. C., and Koshak, W. J.: Optimized regional and interannual variability of lightning in a global chemical transport model constrained by LIS/OTD satellite data, J. Geophys. Res. Atmospheres, 117, https://doi.org/10.1029/2012JD017934, 2012.

Nault, B. A., Garland, C., Pusede, S. E., Wooldridge, P. J., Ullmann, K., Hall, S. R., and Cohen, R. C.: Measurements of $CH_3O_2NO_2$ in the upper troposphere, Atmospheric Meas. Tech., 8, 987–997, https://doi.org/10.5194/amt-8-987-2015, 2015.

Nault, Benjamin. A., Garland, C., Wooldridge, P. J., Brune, W. H., Campuzano-Jost, P., Crounse, J. D., Day, D. A., Dibb, J., Hall, S. R., Huey, L. G., Jimenez, J. L., Liu, X., Mao, J., Mikoviny, T., Peischl, J., Pollack, I. B., Ren, X., Ryerson, T. B., Scheuer, E., Ullmann, K., Wennberg, P. O., Wisthaler, A., Zhang, L., and Cohen, R. C.: Observational Constraints on the Oxidation of NO_x in the Upper Troposphere, J. Phys. Chem. A, 120, 1468–1478, https://doi.org/10.1021/acs.jpca.5b07824, 2016.

Ossohou, M., Galy-Lacaux, C., Yoboué, V., Hickman, J. E., Gardrat, E., Adon, M., Darras, S., Laouali, D., Akpo, A., Ouafo, M., Diop, B., and Opepa, C.: Trends and seasonal variability of atmospheric NO_2 and HNO_3 concentrations across three major African biomes inferred from long-term series of ground-based and satellite measurements, Atmos. Environ., 207, 148–166, https://doi.org/10.1016/j.atmosenv.2019.03.027, 2019.

Petzold, A., Thouret, V., Gerbig, C., Zahn, A., Brenninkmeijer, C. A. M., Gallagher, M., Hermann, M., Pontaud, M., Ziereis, H., Boulanger, D., Marshall, J., Nédélec, P., Smit, H. G. J., Friess, U., Flaud, J.-M., Wahner, A., Cammas, J.-P., Volz-Thomas,

775 A., and Team, I.: Global-scale atmosphere monitoring by in-service aircraft – current achievements and future prospects of the European Research Infrastructure IAGOS, Tellus B Chem. Phys. Meteorol., 67, 28452, https://doi.org/10.3402/tellusb.v67.28452, 2015.

Pickering, K. E., Wang, Y., Tao, W.-K., Price, C., and Müller, J.-F.: Vertical distributions of lightning NO_x for use in regional and global chemical transport models, J. Geophys. Res. Atmospheres, 103, 31203–31216, https://doi.org/10.1029/98JD02651, 780 1998.

Pinardi, G., Van Roozendael, M., Hendrick, F., Theys, N., Abuhassan, N., Bais, A., Boersma, F., Cede, A., Chong, J., Donner, S., Drosoglou, T., Dzhola, A., Eskes, H., Frieß, U., Granville, J., Herman, J. R., Holla, R., Hovila, J., Irie, H., Kanaya, Y., Karagkiozidis, D., Kouremeti, N., Lambert, J.-C., Ma, J., Peters, E., Piters, A., Postylyakov, O., Richter, A., Remmers, J., Takashima, H., Tiefengraber, M., Valks, P., Vlemmix, T., Wagner, T., and Wittrock, F.: Validation of tropospheric NO_2 785 column measurements of GOME-2A and OMI using MAX-DOAS and direct sun network observations, Atmospheric Meas. Tech., 13, 6141–6174, https://doi.org/10.5194/amt-13-6141-2020, 2020.

Poulida, O., Dickerson, R. R., and Heymsfield, A.: Stratosphere-troposphere exchange in a midlatitude mesoscale convective complex: 1. Observations, J. Geophys. Res. Atmospheres, 101, 6823–6836, https://doi.org/10.1029/95JD03523, 1996.

Reed, C., Evans, M. J., Di Carlo, P., Lee, J. D., and Carpenter, L. J.: Interferences in photolytic NO_2 measurements: explanation 790 for an apparent missing oxidant?, Atmospheric Chem. Phys., 16, 4707–4724, https://doi.org/10.5194/acp-16-4707-2016, 2016.

Romer, P. S., Wooldridge, P. J., Crounse, J. D., Kim, M. J., Wennberg, P. O., Dibb, J. E., Scheuer, E., Blake, D. R., Meinardi, S., Brosius, A. L., Thames, A. B., Miller, D. O., Brune, W. H., Hall, S. R., Ryerson, T. B., and Cohen, R. C.: Constraints on Aerosol Nitrate Photolysis as a Potential Source of HONO and NO_x, Environ. Sci. Technol., 52, 13738–13746, https://doi.org/10.1021/acs.est.8b03861, 2018.

795 Ryan, R. G., Marais, E. A., Gershenson-Smith, E., Ramsay, R., Muller, J.-P., Tirpitz, J.-L., and Frieß, U.: Measurement report: MAX-DOAS measurements characterise Central London ozone pollution episodes during 2022 heatwaves, Atmospheric Chem. Phys., 23, 7121–7139, https://doi.org/10.5194/acp-23-7121-2023, 2023.

Ryerson, T. B., Williams, E. J., and Fehsenfeld, F. C.: An efficient photolysis system for fast-response NO_2 measurements, J. Geophys. Res. Atmospheres, 105, 26447–26461, https://doi.org/10.1029/2000JD900389, 2000.

800 Sahu, L. K. and Sheel, V.: Spatio-temporal variation of biomass burning sources over South and Southeast Asia, J. Atmospheric Chem., 71, 1–19, https://doi.org/10.1007/s10874-013-9275-4, 2014.

Scharko, N. K., Berke, A. E., and Raff, J. D.: Release of Nitrous Acid and Nitrogen Dioxide from Nitrate Photolysis in Acidic Aqueous Solutions, Environ. Sci. Technol., 48, 11991–12001, https://doi.org/10.1021/es503088x, 2014.

Schreier, S. F., Peters, E., Richter, A., Lampel, J., Wittrock, F., and Burrows, J. P.: Ship-based MAX-DOAS measurements of 805 tropospheric NO_2 and SO_2 in the South China and Sulu Sea, Atmos. Environ., 102, 331–343, https://doi.org/10.1016/j.atmosenv.2014.12.015, 2015.

SEAC4RS Science Team: SEAC4RS Field Campaign Data, https://doi.org/10.5067/AIRCRAFT/SEAC4RS/AEROSOL-TRACEGAS-CLOUD, 2014.

Sen, P. K.: Estimates of the Regression Coefficient Based on Kendall's Tau, J. Am. Stat. Assoc., 63, 1379–1389, 810 https://doi.org/10.1080/01621459.1968.10480934, 1968.

Shah, V., Jacob, D. J., Dang, R., Lamsal, L. N., Strode, S. A., Steenrod, S. D., Boersma, K. F., Eastham, S. D., Fritz, T. M., Thompson, C., Peischl, J., Bourgeois, I., Pollack, I. B., Nault, B. A., Cohen, R. C., Campuzano-Jost, P., Jimenez, J. L., Andersen, S. T., Carpenter, L. J., Sherwen, T., and Evans, M. J.: Nitrogen oxides in the free troposphere: implications for tropospheric oxidants and the interpretation of satellite NO_2 measurements, Atmospheric Chem. Phys., 23, 1227–1257, https://doi.org/10.5194/acp-23-1227-2023, 2023.

Silvern, R. F., Jacob, D. J., Travis, K. R., Sherwen, T., Evans, M. J., Cohen, R. C., Laughner, J. L., Hall, S. R., Ullmann, K., Crounse, J. D., Wennberg, P. O., Peischl, J., and Pollack, I. B.: Observed NO/NO_2 Ratios in the Upper Troposphere Imply Errors in NO-NO_2-O_3 Cycling Kinetics or an Unaccounted NO_x Reservoir, Geophys. Res. Lett., 45, 4466–4474, https://doi.org/10.1029/2018GL077728, 2018.

Singh, H. B., Thompson, A. M., and Schlager, H.: SONEX airborne mission and coordinated POLINAT-2 activity: Overview and accomplishments, Geophys. Res. Lett., 26, 3053–3056, https://doi.org/10.1029/1999GL900588, 1999.

Singh, H. B., Brune, W. H., Crawford, J. H., Jacob, D. J., and Russell, P. B.: Overview of the summer 2004 Intercontinental Chemical Transport Experiment–North America (INTEX-A), J. Geophys. Res., 111, D24S01, https://doi.org/10.1029/2006JD007905, 2006.

Singh, H. B., Brune, W. H., Crawford, J. H., Flocke, F., and Jacob, D. J.: Chemistry and transport of pollution over the Gulf of Mexico and the Pacific: spring 2006 INTEX-B campaign overview and first results, Atmospheric Chem. Phys., 9, 2301–2318, https://doi.org/10.5194/acp-9-2301-2009, 2009.

Stettler, M. E. J., Eastham, S., and Barrett, S. R. H.: Air quality and public health impacts of UK airports. Part I: Emissions, Atmos. Environ., 45, 5415–5424, https://doi.org/10.1016/j.atmosenv.2011.07.012, 2011.

Stratmann, G., Ziereis, H., Stock, P., Brenninkmeijer, C. A. M., Zahn, A., Rauthe-Schöch, A., Velthoven, P. V., Schlager, H., and Volz-Thomas, A.: NO and NO_y in the upper troposphere: Nine years of CARIBIC measurements onboard a passenger aircraft, Atmos. Environ., 133, 93–111, https://doi.org/10.1016/j.atmosenv.2016.02.035, 2016.

Theil, H.: A Rank-Invariant Method of Linear and Polynomial Regression Analysis, Indag. Math., 12, 1950.

Thompson, C. R., Wofsy, S. C., Prather, M. J., Newman, P. A., Hanisco, T. F., Ryerson, T. B., Fahey, D. W., Apel, E. C., Brock, C. A., Brune, W. H., Froyd, K., Katich, J. M., Nicely, J. M., Peischl, J., Ray, E., Veres, P. R., Wang, S., Allen, H. M., Asher, E., Bian, H., Blake, D., Bourgeois, I., Budney, J., Bui, T. P., Butler, A., Campuzano-Jost, P., Chang, C., Chin, M., Commane, R., Correa, G., Crounse, J. D., Daube, B., Dibb, J. E., DiGangi, J. P., Diskin, G. S., Dollner, M., Elkins, J. W., Fiore, A. M., Flynn, C. M., Guo, H., Hall, S. R., Hannun, R. A., Hills, A., Hintsa, E. J., Hodzic, A., Hornbrook, R. S., Huey, L. G., Jimenez, J. L., Keeling, R. F., Kim, M. J., Kupc, A., Lacey, F., Lait, L. R., Lamarque, J.-F., Liu, J., McKain, K., Meinardi, S., Miller, D. O., Montzka, S. A., Moore, F. L., Morgan, E. J., Murphy, D. M., Murray, L. T., Nault, B. A., Neuman, J. A., Nguyen, L., Gonzalez, Y., Rollins, A., Rosenlof, K., Sargent, M., Schill, G., Schwarz, J. P., Clair, J. M. St., Steenrod, S. D., Stephens, B. B., Strahan, S. E., Strode, S. A., Sweeney, C., Thames, A. B., Ullmann, K., Wagner, N., Weber, R., Weinzierl, B., Wennberg, P. O., Williamson, C. J., Wolfe, G. M., and Zeng, L.: The NASA Atmospheric Tomography (ATom) Mission: Imaging the Chemistry of the Global Atmosphere, Bull. Am. Meteorol. Soc., 103, E761–E790, https://doi.org/10.1175/BAMS-D-20-0315.1, 2022.

Toon, O. B., Maring, H., Dibb, J., Ferrare, R., Jacob, D. J., Jensen, E. J., Luo, Z. J., Mace, G. G., Pan, L. L., Pfister, L., Rosenlof, K. H., Redemann, J., Reid, J. S., Singh, H. B., Thompson, A. M., Yokelson, R., Minnis, P., Chen, G., Jucks, K. W., and Pszenny, A.: Planning, implementation, and scientific goals of the Studies of Emissions and Atmospheric Composition, Clouds and Climate Coupling by Regional Surveys ($SEAC^4RS$) field mission, J. Geophys. Res. Atmospheres, 121, 4967–5009, https://doi.org/10.1002/2015JD024297, 2016.

Torres, O., Bhartia, P. K., Jethva, H., and Ahn, C.: Impact of the ozone monitoring instrument row anomaly on the long-term record of aerosol products, Atmospheric Meas. Tech., 11, 2701–2715, https://doi.org/10.5194/amt-11-2701-2018, 2018.

Travis, K. R., Jacob, D. J., Fisher, J. A., Kim, P. S., Marais, E. A., Zhu, L., Yu, K., Miller, C. C., Yantosca, R. M., Sulprizio, M. P., Thompson, A. M., Wennberg, P. O., Crounse, J. D., St. Clair, J. M., Cohen, R. C., Laughner, J. L., Dibb, J. E., Hall, S. R., Ullmann, K., Wolfe, G. M., Pollack, I. B., Peischl, J., Neuman, J. A., and Zhou, X.: Why do models overestimate surface ozone in the Southeast United States?, Atmospheric Chem. Phys., 16, 13561–13577, https://doi.org/10.5194/acp-16-13561-2016, 2016.

Travis, K. R., Heald, C. L., Allen, H. M., Apel, E. C., Arnold, S. R., Blake, D. R., Brune, W. H., Chen, X., Commane, R., Crounse, J. D., Daube, B. C., Diskin, G. S., Elkins, J. W., Evans, M. J., Hall, S. R., Hintsa, E. J., Hornbrook, R. S., Kasibhatla, P. S., Kim, M. J., Luo, G., McKain, K., Millet, D. B., Moore, F. L., Peischl, J., Ryerson, T. B., Sherwen, T., Thames, A. B., Ullmann, K., Wang, X., Wennberg, P. O., Wolfe, G. M., and Yu, F.: Constraining remote oxidation capacity with ATom observations, Atmospheric Chem. Phys., 20, 7753–7781, https://doi.org/10.5194/acp-20-7753-2020, 2020.

Van Der Velde, I. R., Van Der Werf, G. R., Houweling, S., Eskes, H. J., Veefkind, J. P., Borsdorff, T., and Aben, I.: Biomass burning combustion efficiency observed from space using measurements of CO and NO_2 by the TROPOspheric Monitoring Instrument (TROPOMI), Atmospheric Chem. Phys., 21, 597–616, https://doi.org/10.5194/acp-21-597-2021, 2021.

Van Der Werf, G. R., Randerson, J. T., Giglio, L., Collatz, G. J., Kasibhatla, P. S., and Arellano, A. F.: Interannual variability in global biomass burning emissions from 1997 to 2004, Atmospheric Chem. Phys., 6, 3423–3441, https://doi.org/10.5194/acp-6-3423-2006, 2006.

Van Geffen, J., Eskes, H., Compernolle, S., Pinardi, G., Verhoelst, T., Lambert, J.-C., Sneep, M., Ter Linden, M., Ludewig, A., Boersma, K. F., and Veefkind, J. P.: Sentinel-5P TROPOMI NO_2 retrieval: impact of version v2.2 improvements and comparisons with OMI and ground-based data, Atmospheric Meas. Tech., 15, 2037–2060, https://doi.org/10.5194/amt-15-2037-2022, 2022.

Verhoelst, T., Compernolle, S., Pinardi, G., Lambert, J.-C., Eskes, H. J., Eichmann, K.-U., Fjæraa, A. M., Granville, J., Niemeijer, S., Cede, A., Tiefengraber, M., Hendrick, F., Pazmiño, A., Bais, A., Bazureau, A., Boersma, K. F., Bognar, K., Dehn, A., Donner, S., Elokhov, A., Gebetsberger, M., Goutail, F., Grutter de la Mora, M., Gruzdev, A., Gratsea, M., Hansen, G. H., Irie, H., Jepsen, N., Kanaya, Y., Karagkiozidis, D., Kivi, R., Kreher, K., Levelt, P. F., Liu, C., Müller, M., Navarro Comas, M., Piters, A. J. M., Pommereau, J.-P., Portafaix, T., Prados-Roman, C., Puentedura, O., Querel, R., Remmers, J., Richter, A., Rimmer, J., Rivera Cárdenas, C., Saavedra de Miguel, L., Sinyakov, V. P., Stremme, W., Strong, K., Van Roozendael, M., Veefkind, J. P., Wagner, T., Wittrock, F., Yela González, M., and Zehner, C.: Ground-based validation of the Copernicus Sentinel-5P TROPOMI NO_2 measurements with the NDACC ZSL-DOAS, MAX-DOAS and Pandonia global networks, Atmospheric Meas. Tech., 14, 481–510, https://doi.org/10.5194/amt-14-481-2021, 2021.

Vinken, G. C. M., Boersma, K. F., van Donkelaar, A., and Zhang, L.: Constraints on ship NO_x emissions in Europe using GEOS-Chem and OMI satellite NO_2 observations, Atmospheric Chem. Phys., 14, 1353–1369, https://doi.org/10.5194/acp-14-1353-2014, 2014.

Vohra, K., Marais, E. A., Bloss, W. J., Schwartz, J., Mickley, L. J., Van Damme, M., Clarisse, L., and Coheur, P.-F.: Rapid rise in premature mortality due to anthropogenic air pollution in fast-growing tropical cities from 2005 to 2018, Sci. Adv., 8, eabm4435, https://doi.org/10.1126/sciadv.abm4435, 2022.

Wang, P., Stammes, P., Van Der A, R., Pinardi, G., and Van Roozendael, M.: FRESCO+: an improved O_2 A-band cloud retrieval algorithm for tropospheric trace gas retrievals, Atmospheric Chem. Phys., 8, 6565–6576, https://doi.org/10.5194/acp-8-6565-2008, 2008.

Wang, P.-H., Minnis, P., McCormick, M. P., Kent, G. S., and Skeens, K. M.: A 6-year climatology of cloud occurrence frequency from Stratospheric Aerosol and Gas Experiment II observations (1985-1990), J. Geophys. Res. Atmospheres, 101, 29407–29429, https://doi.org/10.1029/96JD01780, 1996.

Wang, Y., Dörner, S., Donner, S., Böhnke, S., De Smedt, I., Dickerson, R. R., Dong, Z., He, H., Li, Z., Li, Z., Li, D., Liu, D., Ren, X., Theys, N., Wang, Y., Wang, Y., Wang, Z., Xu, H., Xu, J., and Wagner, T.: Vertical profiles of NO_2, SO_2, HONO, HCHO, CHOCHO and aerosols derived from MAX-DOAS measurements at a rural site in the central western North China Plain and their relation to emission sources and effects of regional transport, Atmospheric Chem. Phys., 19, 5417–5449, https://doi.org/10.5194/acp-19-5417-2019, 2019.

Weng, H., Lin, J., Martin, R., Millet, D. B., Jaeglé, L., Ridley, D., Keller, C., Li, C., Du, M., and Meng, J.: Global high-resolution emissions of soil NOx, sea salt aerosols, and biogenic volatile organic compounds, Sci. Data, 7, 148, https://doi.org/10.1038/s41597-020-0488-5, 2020.

van der Werf, G. R., Randerson, J. T., Giglio, L., van Leeuwen, T. T., Chen, Y., Rogers, B. M., Mu, M., van Marle, M. J. E., Morton, D. C., Collatz, G. J., Yokelson, R. J., and Kasibhatla, P. S.: Global fire emissions estimates during 1997–2016, Earth Syst. Sci. Data, 9, 697–720, https://doi.org/10.5194/essd-9-697-2017, 2017.

Wild, O., Prather, M. J., and Akimoto, H.: Indirect long-term global radiative cooling from NOx Emissions, Geophys. Res. Lett., 28, 1719–1722, https://doi.org/10.1029/2000GL012573, 2001.

Yang, L. H., Jacob, D. J., Colombi, N. K., Zhai, S., Bates, K. H., Shah, V., Beaudry, E., Yantosca, R. M., Lin, H., Brewer, J. F., Chong, H., Travis, K. R., Crawford, J. H., Lamsal, L. N., Koo, J.-H., and Kim, J.: Tropospheric NO_2 vertical profiles over South Korea and their relation to oxidant chemistry: implications for geostationary satellite retrievals and the observation of NO_2 diurnal variation from space, Atmospheric Chem. Phys., 23, 2465–2481, https://doi.org/10.5194/acp-23-2465-2023, 2023.

Ye, C., Zhang, N., Gao, H., and Zhou, X.: Photolysis of Particulate Nitrate as a Source of HONO and NOx, Environ. Sci. Technol., 51, 6849–6856, https://doi.org/10.1021/acs.est.7b00387, 2017.

Zhao, B., Wang, S. X., Liu, H., Xu, J. Y., Fu, K., Klimont, Z., Hao, J. M., He, K. B., Cofala, J., and Amann, M.: NOx emissions in China: historical trends and future perspectives, Atmospheric Chem. Phys., 13, 9869–9897, https://doi.org/10.5194/acp-13-9869-2013, 2013.

Ziemke, J. R., Chandra, S., and Bhartia, P. K.: "Cloud slicing": A new technique to derive upper tropospheric ozone from satellite measurements, J. Geophys. Res. Atmospheres, 106, 9853–9867, https://doi.org/10.1029/2000JD900768, 2001.

Zien, A. W., Richter, A., Hilboll, A., Blechschmidt, A.-M., and Burrows, J. P.: Systematic analysis of tropospheric NO_2 long-range transport events detected in GOME-2 satellite data, Atmospheric Chem. Phys., 14, 7367–7396, https://doi.org/10.5194/acp-14-7367-2014, 2014.